

Article

Evaluation of Various Resolution DEMs in Flood Risk Assessment and Practical Rules for Flood Mapping in Data-Scarce Geospatial Areas: A Case Study in Thessaly, Greece

Nikolaos Xafoulis ^{1,*}, Yiannis Kontos ^{2,*}, Evangelia Farsirotou ¹, Spyridon Kotsopoulos ³,
Konstantinos Perifanos ⁴, Nikolaos Alamanis ⁵, Dimitrios Dedousis ⁶ and Konstantinos Katsifarakis ²

¹ Laboratory of Ecohydraulics & Inland Water Management, Department of Ichthyology and Aquatic Environment, University of Thessaly, 38446 Volos, Greece; efars@uth.gr

² School of Civil Engineering, Aristotle University of Thessaloniki, 54124 Thessaloniki, Greece; klkats@civil.auth.gr

³ Department of Energy Systems, University of Thessaly, 41500 Larissa, Greece; kotsopoulos@uth.gr

⁴ Department of Language and Linguistics, National and Kapodistrian University of Athens, 10679 Athens, Greece; kperifanos@phil.uoa.gr

⁵ Department of Agrotechnology, University of Thessaly, 41500 Larissa, Greece; alam@uth.gr

⁶ Department of Civil Engineering, University of Thessaly, 38334 Volos, Greece; ddedousis@uth.gr

* Correspondence: nxafoulis@uth.gr (N.X.); ykontos@civil.auth.gr (Y.K.)

Abstract: Floods are lethal and destructive natural hazards. The Mediterranean, including Greece, has recently experienced many flood events (e.g., Medicanes Zorbas and Ianos), while climate change results in more frequent and intense flood events. Accurate flood mapping in river areas is crucial for flood risk assessment, planning mitigation measures, protecting existing infrastructure, and sustainable planning. The accuracy of results is affected by all simplifying assumptions concerning the conceptual and numerical model implemented and the quality of geospatial data used (Digital Terrain Models—DTMs). The current research investigates flood modelling sensitivity against geospatial data accuracy using the following DTM resolutions in a mountainous river sub-basin of Thessaly's Water District (Greece): (a) open 5 m and (b) 2 m data from Hellenic Cadastre (HC) and (c) 0.05 m data from an Unmanned Aerial Vehicle (UAV) topographical mission. RAS-Mapper and HEC-RAS are used for 1D (steady state) hydraulic simulation regarding a 1000-year return period. Results include flood maps and cross section-specific flow characteristics. They are analysed in a graphical flood map-based empirical fashion, whereas a statistical analysis based on the correlation matrix and a more sophisticated Machine Learning analysis based on the interpretation of nonlinear relationships between input–output variables support and particularise the conclusions in a quantifiable manner.

Keywords: hydraulic simulation; flood maps; digital elevation model; random forests; UAV mapping; DEM sensitivity; DEM errors; HEC-RAS; flood extent; flood risk assessment



Citation: Xafoulis, N.; Kontos, Y.; Farsirotou, E.; Kotsopoulos, S.; Perifanos, K.; Alamanis, N.; Dedousis, D.; Katsifarakis, K. Evaluation of Various Resolution DEMs in Flood Risk Assessment and Practical Rules for Flood Mapping in Data-Scarce Geospatial Areas: A Case Study in Thessaly, Greece. *Hydrology* **2023**, *10*, 91. <https://doi.org/10.3390/hydrology10040091>

Academic Editors: Aristoteles Tegos, Alexandros Ziogas and Vasilis Bellos

Received: 20 March 2023

Revised: 5 April 2023

Accepted: 9 April 2023

Published: 12 April 2023



Copyright: © 2023 by the authors. Licensee MDPI, Basel, Switzerland. This article is an open access article distributed under the terms and conditions of the Creative Commons Attribution (CC BY) license (<https://creativecommons.org/licenses/by/4.0/>).

1. Introduction

Floods are natural disasters that can have severe impacts on human lives, infrastructure, and the environment [1,2]. Floods can occur due to various reasons, such as heavy rainfall, river overflow, coastal storm surges, or tsunamis. The response of mountain basins to intense rainfall is rapid, mainly due to large slopes, while precipitation is spatially and temporally variable [3]. Mountain basin floods are often flashy [4], allowing limited time for warnings. Flash floods usually occur in mountain river catchments draining less than 1000 km² [5]. They constitute a common, extremely dangerous natural hazard and they are responsible for many deaths [6,7]. Their impacts on various socioeconomic activities are extremely diverse [8,9]. Around 40% of flood-related deaths in Europe between 1950 and 2006 are linked to flash floods [10]; still, there is a lack of relevant data, especially reliable discharge estimates [4]. The Mediterranean region is one of the most flood-prone

areas in the world due to its unique geographic, climatic, and environmental conditions, with floods occurring on average every two years; floods are one of the most lethal and destructive natural hazards [11] there. Greece is also affected by floods that are mainly caused by heavy rainfall (e.g., flood in the city of Karditsa caused by Medicane Ianos [12]), river overflow, and flash floods (e.g., flood in Mandra with 24 fatalities caused by Medicane Numa-Zenon [13]). Greece has also experienced many flood events during the last decades [7].

One of the most effective ways to reduce the impacts of floods is to develop and implement flood management plans that include prevention, preparedness, response, and recovery measures. Flood mapping is a crucial tool for flood management planning as it enables the a priori identification of flood-prone areas, and the estimation of flood extent, flow depth and characteristics, and flood frequency [14]. There are several challenges in modelling floods using informed modelling, such as data quality issues, uncertainty in input parameters, and the need for improved model calibration. Flood model parameters are of grey-box nature and their global use is not suggested but rather should be carefully adopted [13]. Moreover, advanced modelling approaches supported by detailed spatial information are not always the answer. They are extremely computationally and data-greedy in order to overcome uncertainties [15]. Most of the time, a compromise between simulation accuracy and time defines the simulation scheme/model used. Hence, 1D flood modelling can be implemented, especially in data-scarce areas. In such cases, open real-world datasets can improve flood modelling [12]. The use of forensic hydrology, reconstructing flood events through field observations, hydrological and hydraulic modelling, and geomorphological analysis, is an established method to overcome the lack of data and provide valuable insights into past events and inform future flood risk management strategies [12].

An essential tool for successful flood risk management is accurate flood mapping. This requires the use of high resolution and accurate Digital Elevation Models (DEMs) [16]. High resolution does not always guarantee DEM accuracy, especially when dense vegetation and canopy are involved and the mapping is based on orthophotos. In such cases, the accuracy also depends on the vegetation filtering techniques used.

Current research investigates flood modelling sensitivity against geospatial data accuracy, in a case study concerning a part of the mountainous Enipeas river basin of Thessaly's Water District (Greece). The methodology that is implemented in the current research is graphically presented step-by-step in Figure 1. In particular, the following DEMs for the study area concerning flood modelling (flood area) are tested: (a) open 5 m resolution DEM data (DEM_5 m) from the Hellenic Cadastre (HC; [17]), (b) open 2 m resolution DEM data (DEM_2 m) from the HC, and (c) sub-meter (0.05 m) resolution DEM data (DEM_0.05 m) from a research team's own designated Unmanned Aerial Vehicle (UAV) topographical mission. The US Army Corps of Engineers' software [18] RAS-Mapper [19] and HEC-RAS 1D [20] are used for 1D (steady state) hydraulic simulations (Sims) regarding a 1000-year return period for the three different DEMs (DEM_5 m = Sim 1; DEM_2 m = Sim 2; DEM_0.05 m = Sim 3). Results include 2D flood maps graphically presenting spatial flood extents and flow depths, as well as flow characteristics for every cross-section of the hydrographic network, such as Froude number, hydraulic radius, and flood extent. In the absence of an ideal terrestrial mapping mission using land-based topographical instruments of the studied hydrographic network, DEM_0.05 m and the resulting hydraulic simulation (Sim 3) are assumed to be the "ground truth". Thus, the investigation focuses on the comparison of the results of the two open data-based simulations, Sim 1 and Sim 2, against the closer to the truth Sim 3 results.

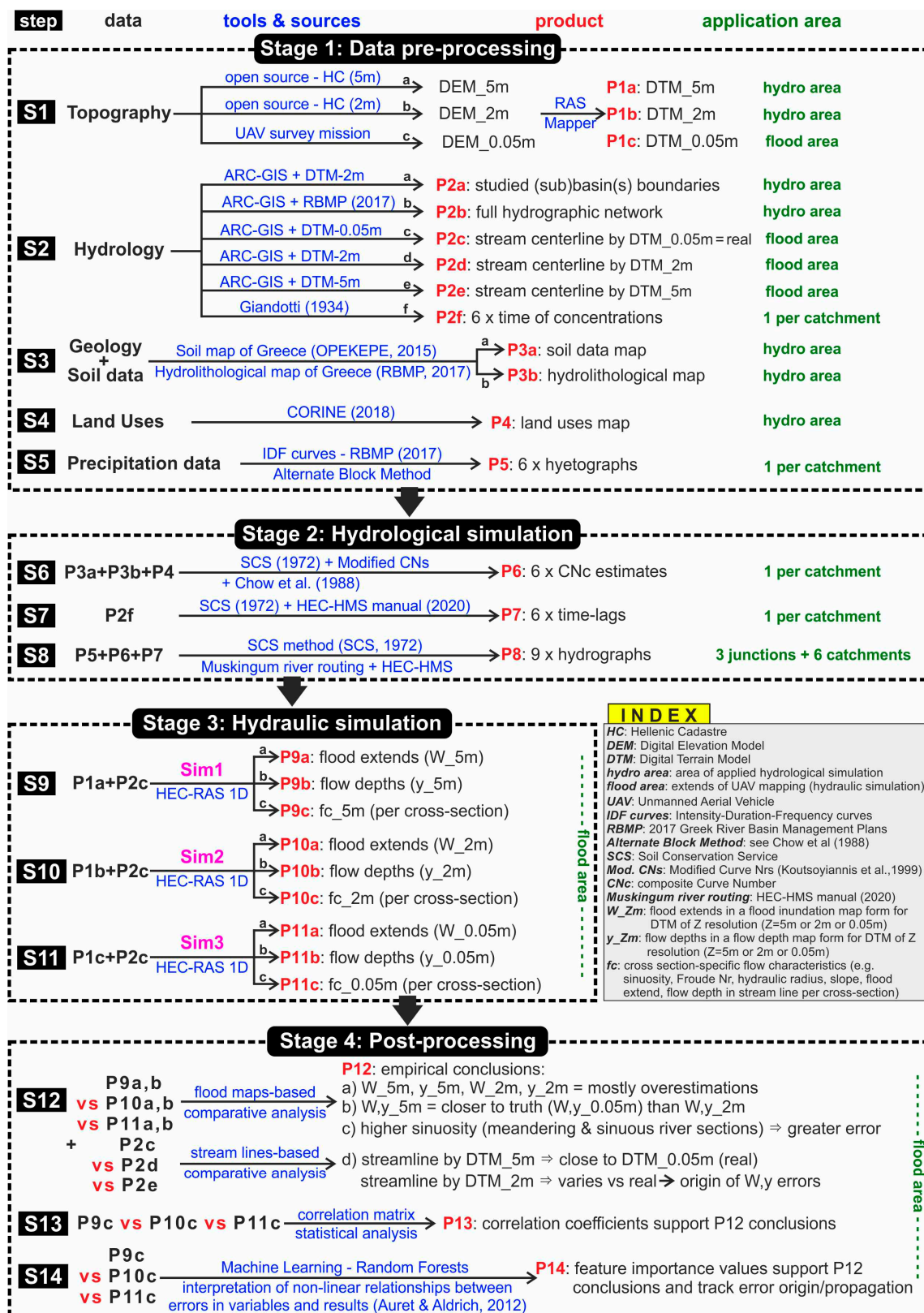


Figure 1. Graphical abstract of the methodology implemented to investigate the sensitivity of flood risk mapping via 1D hydraulic simulations vs. various DEM resolutions. Aim: conclude on study area features that render the use of more accurate but costly and time-consuming UAV mapping imperative and decide on the next best free alternative option in Greek reality [29,42].

The flood modelling results are analysed in a graphical flood map-based empirical fashion, whereas a statistical analysis, based on the correlation matrix, and a more sophisticated Machine Learning (ML) analysis, support and particularise the conclusions in a quantifiable manner; the ML-assisted analysis is based on the interpretation of the non-linear relationships between input–output variables (i.e., DEM, sinuosity, slope vs. flow extents, flow depths, flow characteristics). The goal is to track the errors in the simulation results and trace them back to the initial features that generated them, in relation to the selected DEM; this way, one can conclude on the features that render the use of the more accurate, but costly and time-consuming, UAV mapping imperative, while deciding on the next best free alternative DEM (5 m or 2 m) option in Greek reality.

The practical aim of this paper is to produce practical rules for optimal hydraulic simulation of a river basin, in terms of minimization of in situ topographical mapping costs without compromising the hydraulic simulation accuracy. This way, one can decide on which hydrographic network sections (if any) of any river basin demand UAV or other accurate mapping or not and what the free alternative is. This requires a transparent and detailed presentation of the implemented and proposed methodology so that the conclusions can be generalized.

2. Materials and Methods

This section presents the study area and all stages of the implemented methodology, with their discrete steps, as presented in the graphical abstract (Figure 1), mentioning all data sources and methods along the way. Stage 1 (see Section 2.2) refers to data pre-processing, including procurement and processing/manipulation of topography, hydrology, geology, soil, land uses, and precipitation data. Stage 2 (see Section 2.3) refers to hydrological simulations, including calculation of hydrological parameters and production of hydrographs, required as input for the hydraulic simulations included in Stage 3. Stage 3 (see Section 2.4) produces 2D flood maps and cross-section-specific results that are analysed in Stage 4 (see Section 2.5) via three different approaches: (a) empirical, (b) statistical, and (c) interpretation of non-linear relationships using Machine Learning.

2.1. Study Area

The Thessaly Water District (EL08; [21]) includes two main river basins: (a) the Pinios river basin and (b) the Almyros-Pilion basin. The study area is located in the district's southern section, being part of the Pinios basin. It specifically lies in the north-west of Mount Othris, being a part of the mountainous river basin of Enipeas river (code GR00080004002203). Figure 2 presents the location of the study area, and the wider study area (where the hydrological simulations are conducted; shortly referred to as “hydro area”) as a part of the Thessaly Water District and the Enipeas river basin. Figure 3 presents the specific study area where the hydraulic simulations are conducted (shortly referred to as “flood area”), as a part of the wider “hydro area”.

2.2. Data Pre-Processing (Methodology Stage 1)

2.2.1. Topographic Data (Step 1)

The geospatial data utilised in this research come from HC [17] and a private UAV mission. DEM_5 m is actually the “Digital Elevation Model-DEM-LSO (5 m)” dataset series, as presented by HC [22], which “is a 5 m pixel size grid compilation (1:5000 cadastral tile distribution), deriving from the Large Scale Orthophotos project. It is a homogenous systematic point grid which refers to terrain elevation and creates an Earth Elevation Model”. RAS-Mapper [19] is used to convert DEM_5 m into DTM_5 m (research product P1a; see Figure 1); the respective map is provided as Appendix A File SM1 (see Appendix A for details).

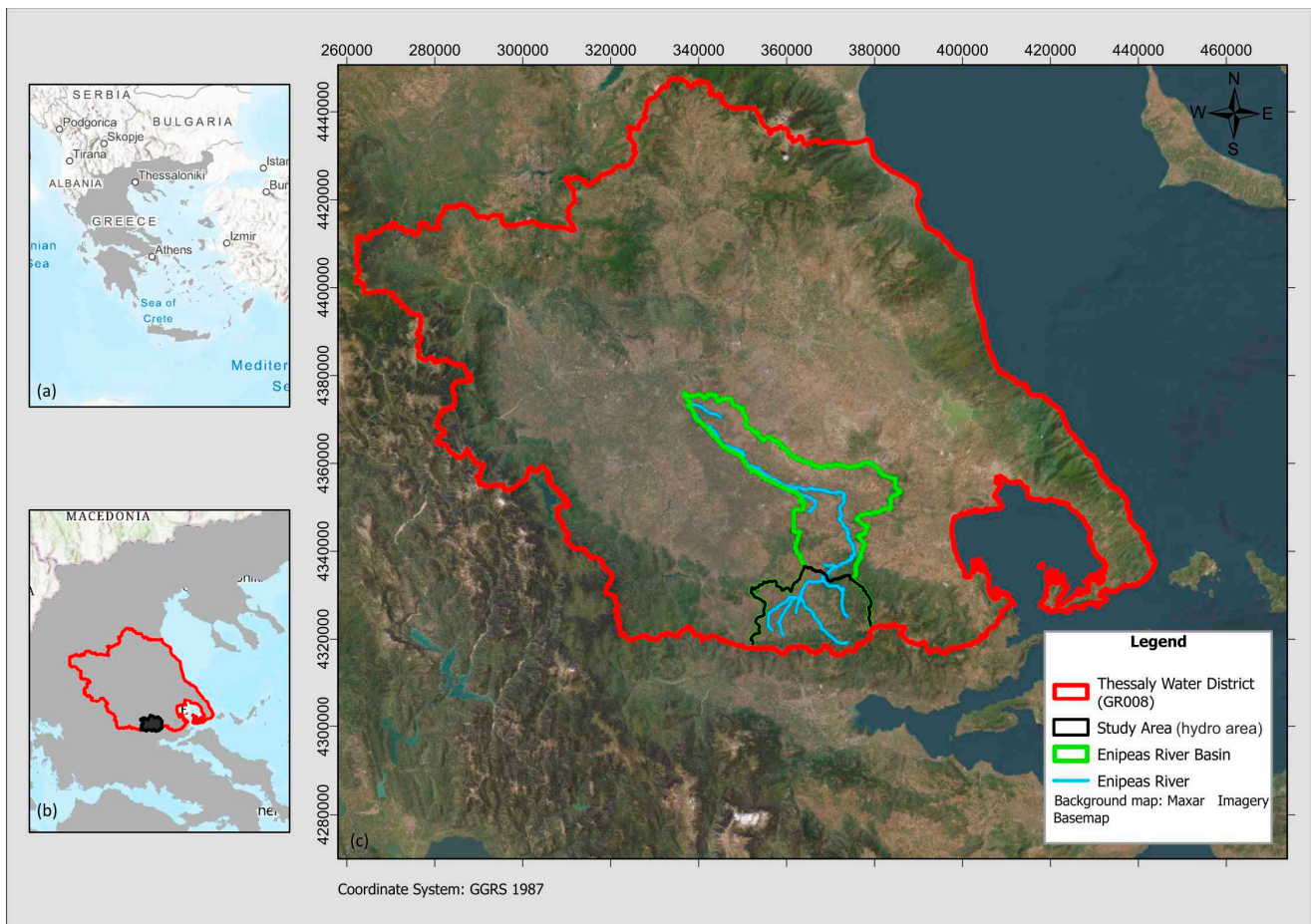


Figure 2. (a) Map of Greece, (b) Thessaly Water District, and (c) Enipeas river basin and wider studied catchment (hydro area) with the studied hydrographic network.

DEM_2 m is actually the “Digital Elevation Model-DEM-LSO25” dataset series as presented by HC [23], which “is a 2 m pixel size grid compilation (1:2500 cadastral tile distribution), for the entire country from airphotos taken between 2014 and 2016, deriving from the Large Scale Orthophotos 25 cm (LSO25) project. It is a homogenous systematic point grid which refers to terrain elevation and creates an Earth Elevation Model”. RAS-Mapper [19] is used to convert DEM_2 m into DTM_2 m (P1b_flood for “flood area” and P1b_hydro for “hydro area”; see SM2a and SM2b, respectively).

DEM_0.05 m is produced by the research team’s own designated UAV topographical mission. Structure-from-Motion (SfM) photogrammetry using photographs obtained by UAVs is increasingly being utilised for producing high resolution DEMs. The UAV used is WingtraOne GEN II. The flight took place on 3 March 2022 and lasted about 20 min to survey the “flood area” of approximately 1.05 km². The DEMs are interpolated from point clouds that represent entire landscapes, including terrain, vegetation, and infrastructure [24]. In the current research, the vegetation filtering is conducted with the standard method of Agisoft Metashape software application [25]. RAS-Mapper [19] is used to convert DEM_0.05 m into DTM_0.05 m (P1c; see SM3). DTM_0.05 is contained within the boundaries of the UAV mapping (DEM_0.05 m) where the hydraulic simulations are conducted (flood area), as presented in Figure 3.

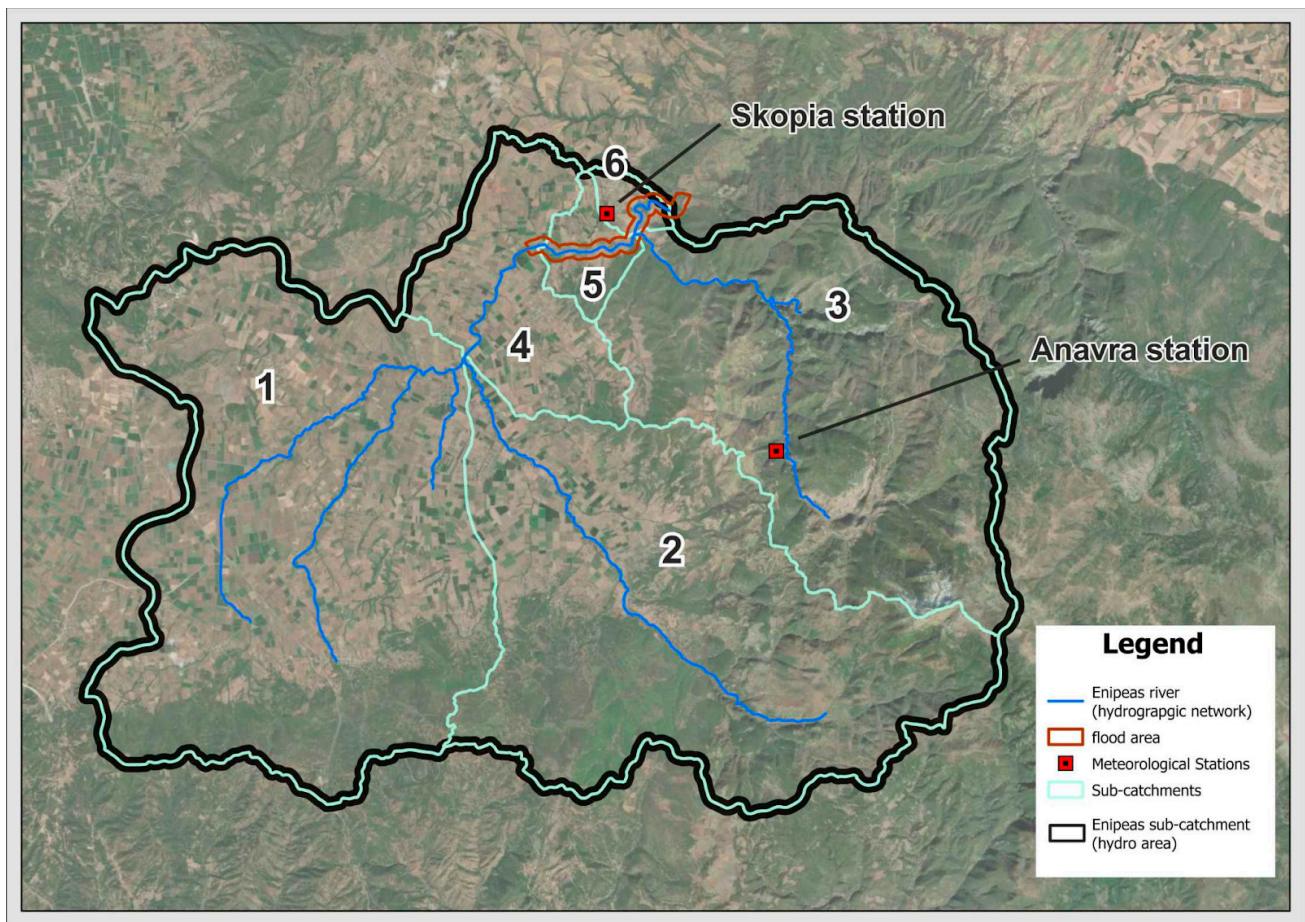


Figure 3. Study area of Enipeas river basin where the hydraulic simulations are conducted (flood area) as a part of the wider study area where the hydrological simulations are conducted (hydro area), together with the hydrographic network, the sub-catchments, and available meteorological stations.

2.2.2. Hydrology-Related Data and Calculations (Step 2)

Using the software ArcGIS Pro v3.1.0 [26], the “hydro” studied area is divided into sub-basins/catchments (P2a; see Figure 3 and SM4) based on DTM_2 m in conjunction with orthophotos derived from HC [23] and satellite images. The finer of the two resolutions available in the wider “hydro” study area DTM_2 m is used, as it allows for a finer representation of the low- and very low-slope areas of the study area, as well as various technical structures such as embankments. Figure 4 presents the “hydro” area, together with the hydrographic network. The latter derives from the River Basin Management Plans of the Water District of Thessaly [27], in conformation with the Water Framework Directive (2000/60/EC; [28]) and comprises the main stream sections of Enipeas hydrographic network (P2b; see SM5).

A more accurate stream centerline (part of the hydrographic network in the “flood” area) is also produced in this step (P2c and P2c_DTM; see SM6a,b), derived from the most accurate DTM_0.05 m. This will be used for the hydraulic simulation. Moreover, although not needed for the simulations, the respective stream centerlines derived from DTM_5 m (P2d and P2d_DTM; see SM7a,b) and DTM_2 m (P2e and P2e_DTM; see SM8a,b) are produced to be used for comparison and deduction of conclusions in the last section of the paper. All stream lines are produced using ArcGIS Pro. All of the geomorphological characteristics of the sub-catchments of the “hydro” area are presented in Table 1. Step 2 ultimately features use of the Giandotti methodology [29] for the calculation of the six concentration times (Table 1), one per sub-catchment (P2f; see SM9).

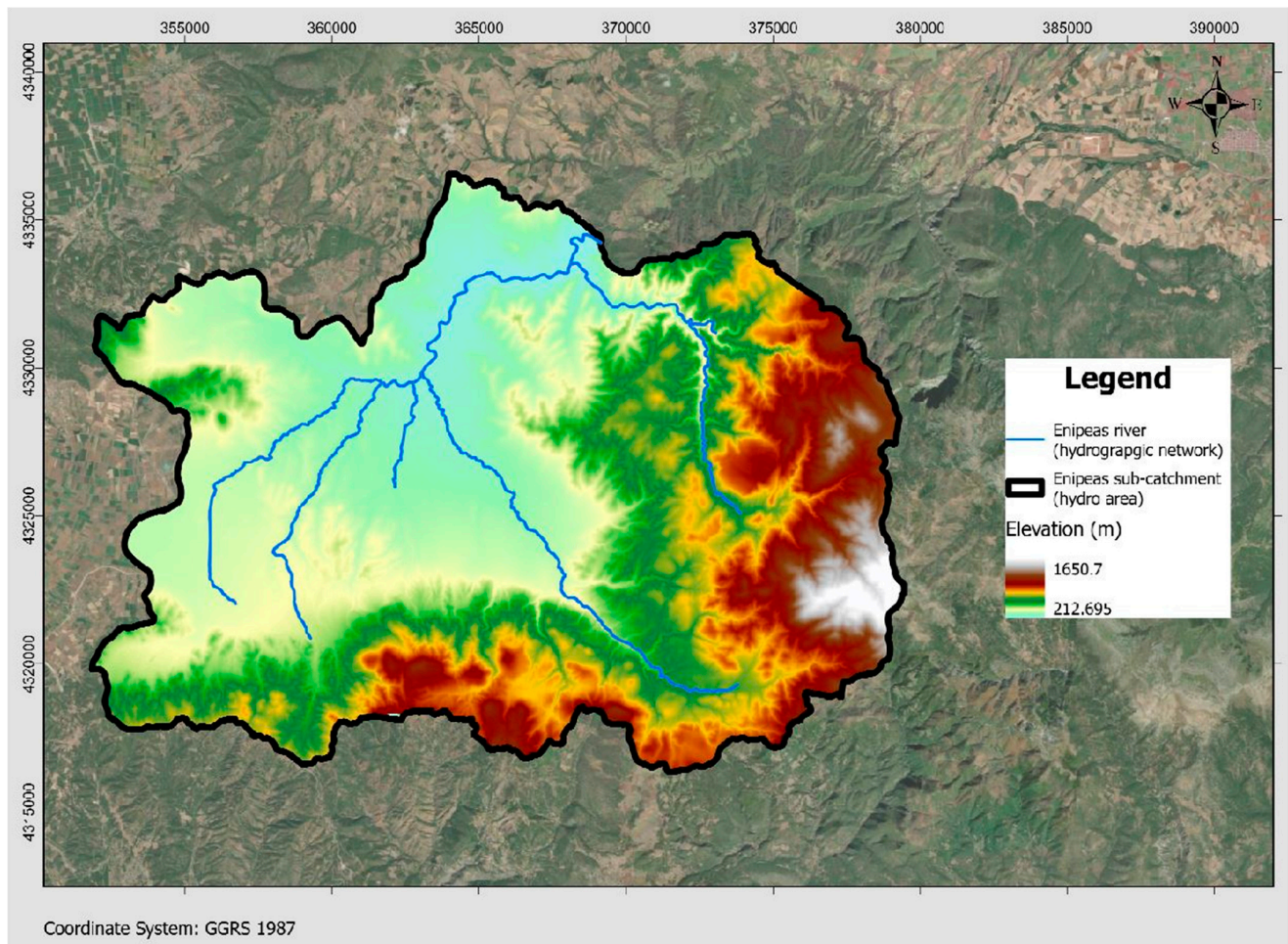


Figure 4. Digital Terrain Model of 2 m × 2 m resolution (DTM_2 m) of the study area (“hydro”) used for the delineation of the sub-catchments and hydrographic network (see SM2a and SM5).

Table 1. The geomorphological features of all sub-catchment areas, together with the respective concentration times, lag times, and Areal Reduction factor (ARF).

Sub-Catchment	Area (km ²)	Length of Main River (km)	Mean Sub. Elevation (m)	Outlet Elevation (m)	Time of Concentration (h)	Lag Time (h)	Areal Reduction Factor	CNc
Sub 1	141.21	14.339	538.95	375.00	6.74	4.04	0.89	71
Sub 2	121.68	17.867	731.95	375.00	4.69	2.81	0.88	71
Sub 3	96.26	13.416	842.28	344.73	3.33	2.00	0.87	55
Sub 4	30.30	8.362	426.47	360.23	5.31	3.19	0.92	74
Sub 5	6.72	3.156	416.9	344.72	2.22	1.33	0.93	63
Sub 6	3.19	2.287	397.29	327.23	1.58	0.95	0.94	55

2.2.3. Geological and Soil Data (Step 3)

The most reliable sources for geological/soil data and, consequently, hydrolithological data are the European Soil Data Center (ESDAC) [30–33], the Soil Map of Greece by the Greek Payment Authority of Common Agricultural Policy (OPEKEPE; [34]), and the River Basin Management Plan for the Water District of Thessaly (RBMP-EL08) [27]. The main source of the soil data is OPEKEPE; the available separate soil map tiles are scanned and georeferenced on the “hydro” area using ArcGIS Pro (P3a; see SM10). The soil map does not cover the full extent of the study area. The missing data are drawn by the hydrolithological map provided by RBMP-EL08 [27]. The available data from ESDAC

successfully validate the other sources. The soil types of OPEKEPE are linked to the respective hydromorphy and are categorised into classes (A: high; B: moderate; C: low; D and E: very low infiltration rates), whereas the RBMP map also categorises the soil types concerning the hydrolithological characteristics. The resulting merged hydrolithological map is presented in Figure 5 (P3b; see SM11).

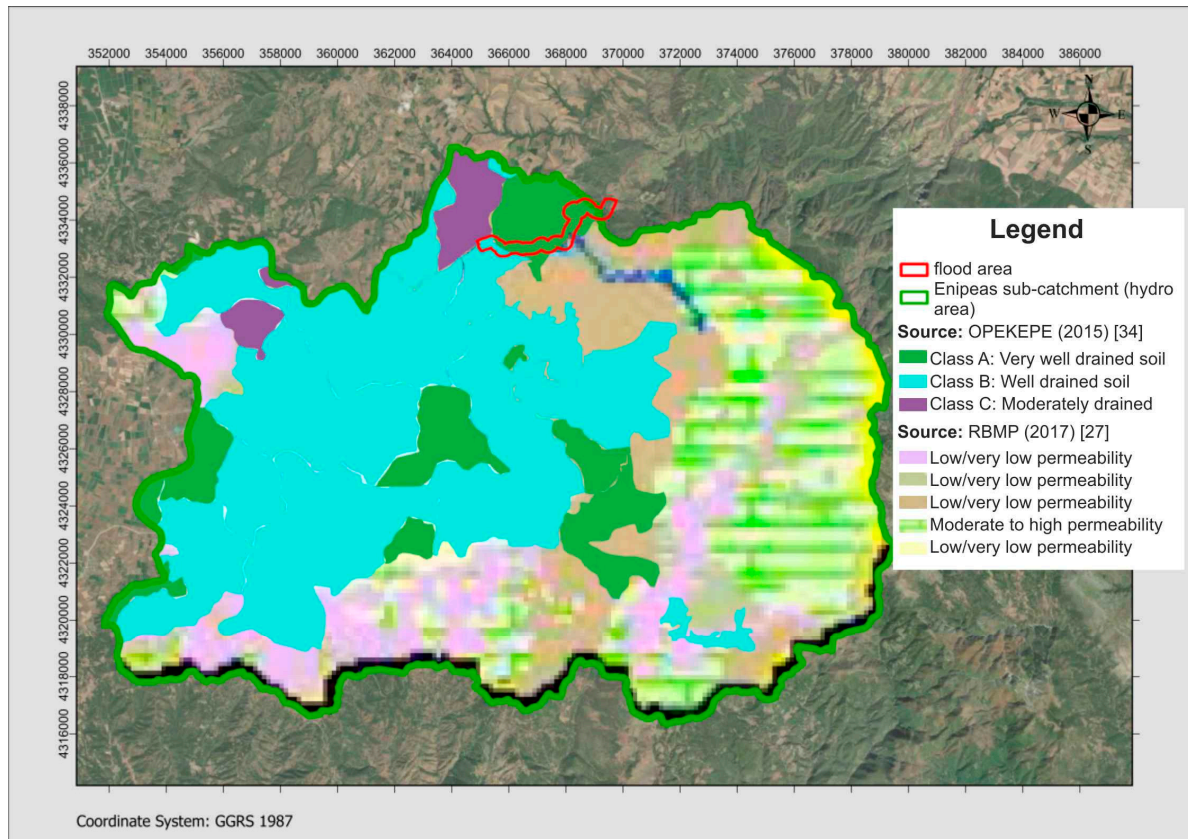


Figure 5. Hydrolithological map of the study area by merged OPEKEPE [34] and RBMP [27] data (see SM11).

2.2.4. Land Use Data (Step 4)

The determination of the land cover was based on CORINE land cover data [35]. The land use map is presented in Figure 6 (P4; see SM12). All information regarding CORINE land cover classes and the respective land cover area per sub-catchment are presented in SM14 (P6).

2.2.5. Precipitation Data Hyetograph Production (Step 5)

The only available meteorological stations in the study area (hydro) are those located at Anavra and Skopia, as presented in Figure 3. In order to be on the safe side and investigate the worst-case scenario regarding rainfall intensity, the higher-elevation Anavra station is selected; it always provides greater precipitation heights. Under these data-scarce conditions, following the methodology by Koutsoyiannis et al. [36], the Intensity Duration Frequency (IDF) curve was designed, using the proposed equation:

$$i(t, T) = \frac{\lambda' \cdot (T^\kappa - \psi')}{(1 + \frac{t}{\theta})^\eta}, \quad (1)$$

where i is the max point rainfall intensity of duration t for a return period of T ; θ and η are parameters to be estimated, with $\theta \geq 0$ (in time units) and $0 < \eta < 1$; $\kappa > 0$ is the shape parameter; $\lambda' > 0$ is the scale parameter; and ψ' is the location parameter.

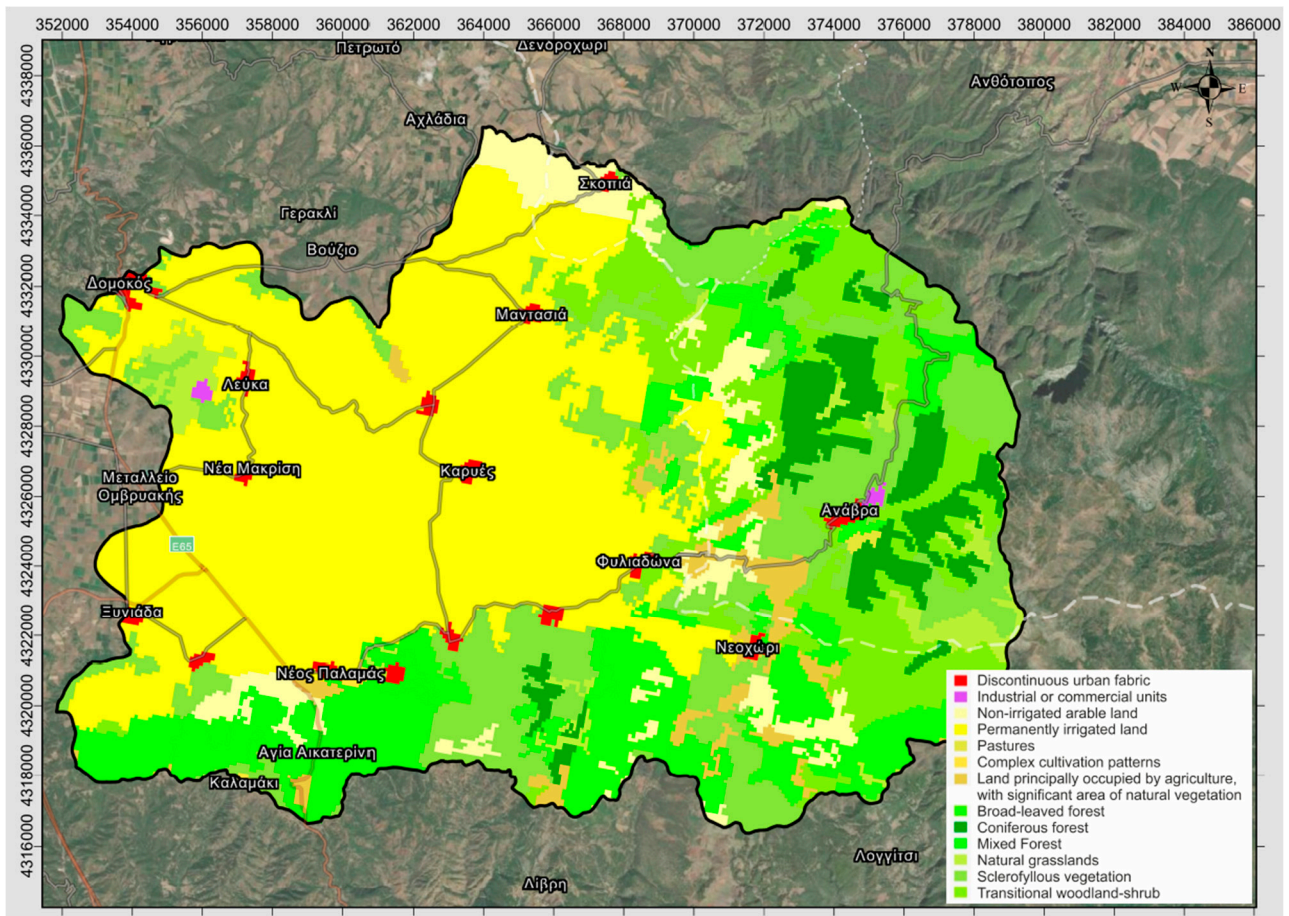


Figure 6. Land use map derived from CORINE [35] (see SM12).

The parameters proposed by the IDF Report v4 [37] (supporting documents of [27]) for the Anavra station and for a return period of 1000 years are presented in Table 2. The resulting function and IDF curve are presented in Figure 7.

Table 2. Parameters used in the IDF curve equation [36], regarding the Anavra station and a 1000-year return period.

Water District Code	Station ID	Station Name	X (m)	Y (m)	Z (m)	κ	λ'	ψ'	θ	n
GR08	355	Anavra	372,326.71	4,327,100.77	208	0.092	592.3	0.768	0.042	0.639

Next, the point rainfall intensity is transformed to areal rainfall intensity using the respective Areal Reduction Factor (ARF) per sub-catchment, calculated by [36,37]:

$$\varphi = \max\left(1 - \frac{0.048 \cdot A^{0.36 - 0.01 \cdot \ln A}}{d^{0.35}}, 0.25\right), \quad (2)$$

where A is the river basin area (km²) and d is the rainfall duration (h).

The ARF values per sub-catchment are presented in Table 1 (sources: [38–41]). The respective design hyetographs per sub-catchment are produced (P5; see SM13) based on the IDF curve using the Alternate Block Method [42,43].

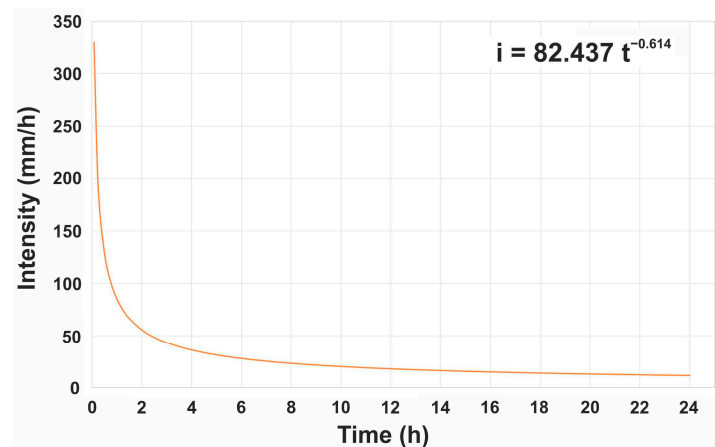


Figure 7. The IDF function and curve (point rainfall intensity vs. time) for the Anavra station for a return period of 1000 years.

2.3. Hydrological Simulation (Methodology Stage 2)

All current hydrological simulations are conducted using the Hydrologic Engineering Center—Hydrologic Modelling System (HEC-HMS), developed by the US Army Corps of Engineers [18]. HEC-HMS is a widely used and established tool that can simulate all hydrological processes of a watershed, including precipitation, infiltration, evaporation, snowmelt, and runoff. It is used for the design and management of water resource infrastructure, such as dams, reservoirs, and water supply systems. The transformation of precipitation into runoff for every sub-catchment was conducted using the Soil Conservation Service—Curve Number (SCS-CN) [44] unit hydrograph method, whereas losses are estimated using the SCS-CN model.

2.3.1. Curve Numbers (Step 6)

SCS-CN is a simple, widely used, and efficient method for determining the amount of runoff from rainfall, even in a particular area. A Curve Number (CN) [42] expresses the percentage of precipitation that will runoff as a function of the area's hydrologic soil group, land use, treatment, and hydrologic condition. Based on Chow et al. (1988; [42]), Koutsoyiannis and Xanthopoulos (1999; [45]) provided updated CN values, used in current research. There are various land uses in every sub-catchment, hence the weighted Curve Number (composite) value CN_c is calculated [46]. The estimation process is presented in SM14, whereas the calculated CN_c values are presented in Table 1.

2.3.2. Lag Time Estimation (Step 7)

Following the SCS methodology [44] and the HEC-HMS Technical Reference manual [47], the lag times for each sub-catchment are estimated (Table 1). Lag time refers to the delay between the occurrence of rainfall and the peak discharge of a river. It depends on size and shape of the catchment, soil type, and vegetation cover.

2.3.3. Hydrograph Production (Step 8)

Following the SCS methodology [44], hydrographs are produced (P8; see SM15) using HEC-HMS, applying the well-established Muskingum river routing method to all reaches. Parameters such as reach length and slope are estimated using topographical data, namely DTM_2 m. The nine hydrographs refer to the three junctions and six sub-catchments created by the studied Enipeas basin (hydro area) model, as presented in Figure 8.

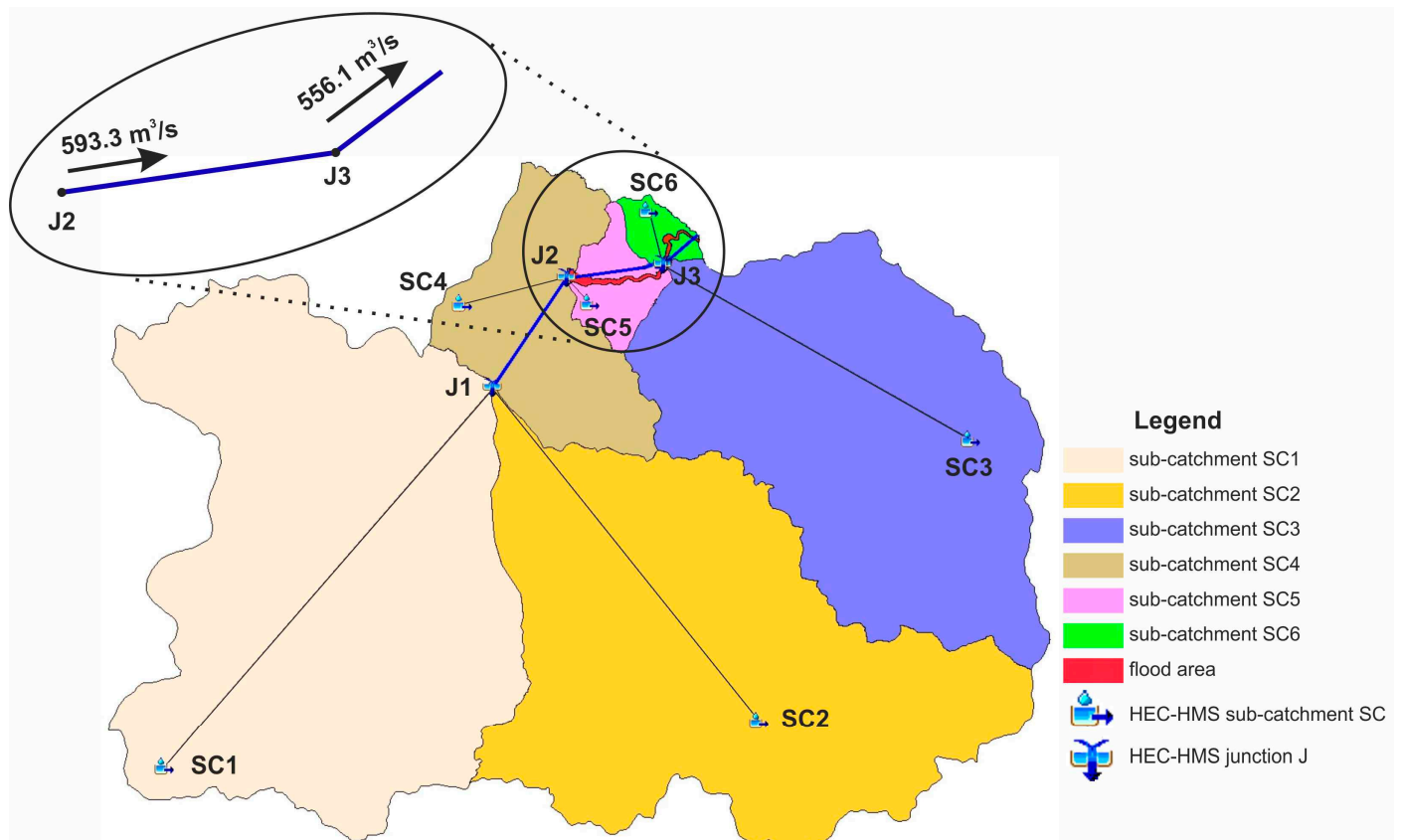


Figure 8. HEC-HMS hydrological model of the studied (hydro) area, featuring its six sub-catchments and three junctions, with detail of the calculated design discharges used in HEC-RAS.

2.4. Hydraulic Simulation (Methodology Stage 3; Steps 9, 10, 11)

All current hydraulic simulations are conducted using the Hydrologic Engineering Center—River Analysis System (HEC-RAS 1D) developed by the US Army Corps of Engineers [48]. It is a powerful tool for hydraulic modelling, based on a 1D numerical system, able to simulate steady/unsteady flow conditions. HEC-RAS can be used for a variety of hydraulic analyses, including floodplain mapping, bridge and culvert design, dam safety evaluations, sediment transport studies, and water quality modelling. The model solves equations for conservation of mass and momentum to calculate water surface elevation, flow velocity, and other hydraulic characteristics. It exhibits a user-friendly interface and features tools such as RAS-Mapper [19], supporting a range of data input formats, including DEMs, topographic maps, and surveyed cross-sections and post-processing utilities for displaying and analysing simulation results.

Although there is only one shared hydrological simulation applied in the wider “hydro” area, there are actually three hydraulic simulations, namely 1D implementations of the HEC-RAS 1D model, corresponding to the three input DTMs applied in the “flood” area: (a) Sim 1 uses DTM_5 m, (b) Sim 2 uses DTM_2 m, and (c) Sim 3 uses DTM_0.05 m. All three Sims share the river centerlines (Step 2; products P2c, P2d, P2e), as well as the bank lines, produced by DTM_0.05 m, which is assumed to be the “ground truth”. Sims 1–3 also share 270 cross-sections positioned in an interval of approximately 20 m along the river centerline (see SM23). For all Sims, two Manning coefficient values are used, one for the main channel ($n = 0.08$) and a different one for the overbanks ($n = 0.07$). The values were decided after observations of satellite images and orthophotos and in situ inspection, based on Chow et al. (1988; [42]) and the HEC-RAS hydraulic reference manual [48]. The values were adjusted, as [42] suggests, based on river irregularities, variation in channel cross-section, obstructions, vegetation, and meandering. The contraction and expansion coefficients for

all Sims are assumed to be equal to 0.1 and 0.3, respectively [48]. The maximum flow (sic.) values in the respective HEC-HMS-produced hydrographs of junctions J2 (539.3 m³/s; see SM15, page 1) and J3 (556.1 m³/s; see SM15, page 3) are used as steady flow discharges in all hydraulic simulations (Figure 8). Concerning upstream and downstream boundary conditions, the energy grade line slope values are assumed to be equal to the riverbed slope values [48].

Step 9 in Stage 2 of the applied methodology features Sim 1, namely HEC-RAS 1D simulation of the hydraulic model based on DTM_5 m, producing the respective W_5 m flood extent map (P9a; see SM16), the respective y_5 m flow depths map (P9b; see SM17), and calculating the flow characteristics. The fc_5 m flow characteristics selected to be investigated for their involvement in the propagation of errors generated by the lower resolution DEMs are presented per cross-section in SM18, including meter mark, hydraulic radius, Froude number, and flood extent.

Step 10 in Stage 2 of the applied methodology features Sim 2, namely HEC-RAS 1D simulation of the hydraulic model based on DTM_2 m, producing the respective W_2 m flood extent map (P10a; see SM19) and the respective y_2 m flow depths map (P10b; see SM20), and calculating the fc_2 m flow characteristics (P10c; see SM18).

Step 11 in Stage 2 of the applied methodology features Sim 3, namely HEC-RAS 1D simulation of the hydraulic model based on DTM_0.05 m produces the respective W_0.05 m flood extent map (P11a; see SM21) and the y_0.05 m flow depths map (P11b; see SM22), and calculating the fc_0.05 m flow characteristics (P11c; see SM18).

2.5. Post-Processing and Analysis (Methodology Stage 4)

Stage 4 features the post-processing of the results of the three hydraulic simulations (Sim 1–3) via (a) empirical (Step 12) and (b) statistical (Step 13) analysis as well as (c) use of Machine Learning for the interpretation of non-linear relationships of variables vs. results (Step 14).

The production of conclusions concerning the free DEMs and the UAV-produced DEM in relation to the hydraulic simulation results requires an initial conventional comparative analysis of the results of the three simulations (Sim 1–3). This demands the post-processing of the results, including graphical representation in the form of comparative maps (i.e., flood extent maps, flow depths maps, and maps with centerlines produced from the various DTMs), for the empirical but informed conclusion production. These are presented and discussed in the “Results and discussion” section (Section 3.1).

These initial conclusions must be supported by a more quantitative statistical analysis of cross-section-specific variables and results. Specifically, the correlation coefficient (Pearson product-moment correlation coefficient), a measure of linear association between two variables, is calculated between all involved input data and variables (Sim/DTM-specific or common for all Sims/DTMs) and results (flood extents, flow depths, flow characteristics). The calculated correlation matrix can be used to support the empirical conclusions of Step 12, but also help explore other patterns, namely the factors that magnify and propagate errors originating from lower resolution DEMs in various sections.

As the investigation process is actually a root cause analysis concerning the impact of the various DEM resolutions on the hydraulic simulation, a more sophisticated method to interpret the nonlinear dependencies between variables and results is needed. A well-documented methodology from Machine Learning, Random Forest (RF) importance [49], is utilised. An interval (t_{lower} , t_{upper}) is defined, where the residuals are reasonably small, and RF is fitted on the residuals that are larger than t_{upper} and lower than t_{lower} , observing the mean node impurity of the forest as a feature importance proxy. The key insight here is to include a gaussian noise “dummy” variable, uncorrelated with the target variable, as an additional feature, which is known to have no impact on the target output. By using the importance of this variable as a baseline, conclusions can be drawn on the importance of the other variables that have larger importance compared to the “dummy” variable, also including the error bars. This implementation should overcome the

theoretical weakness of the statistically limited dataset, due to the study of a geospatially data-scarce area.

3. Results and Discussion

3.1. Comparative Analysis Based on Produced Maps (Step 12)

The production of empirical conclusions is mainly based on the comparative analysis of flood extent and flow depth maps. Figure 9 presents the flood extents for all three Sims projected on the same map (see SM24). It includes the five identified river sections exhibiting different sinuosity ratios (SR) in order to investigate the possible correlation between SR and simulation errors in lower resolution Sims 1 and 2. For a finer, more detailed comparison of the flood extent maps' differences, comparative maps for all combinations are available as Appendix A (SM25: W_5 m vs. W_0.05 m; SM26: W_2 m vs. W_0.05 m; SM27: W_5 m vs. W_2 m). The red line, representing the UAV-produced flood extents of Sim 3 (W_0.05 m) is assumed to be the "ground truth", namely the closest to the truth available flood extents (inundated area = 0.7 km²). Although Sim 1 and Sim 2 flood extents (W_5 m and W_2 m, respectively) constitute reliable simulations and provide satisfactory approximations, there are many errors, as presented in Tables 3 and 4. Inundation areas produced by Sim 1 and Sim 2 are 0.836 km² and 0.896 km², respectively. Most of the errors are overestimations rather than underestimations (Table 3), at least being on the safe side.

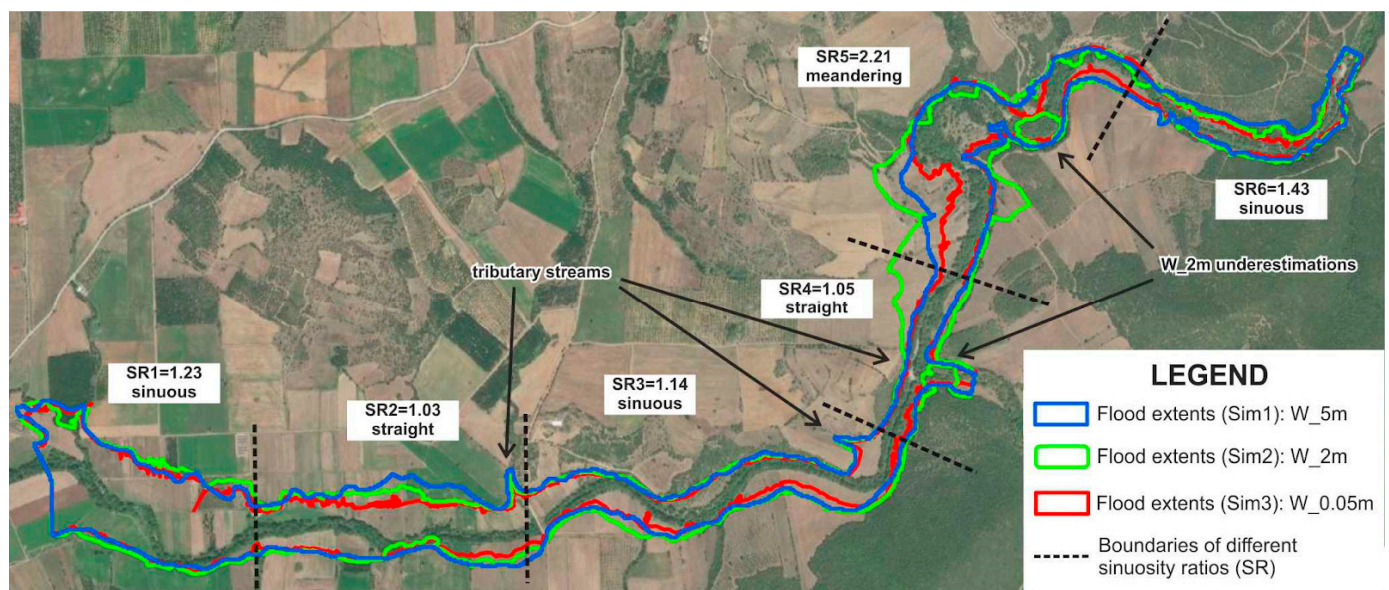


Figure 9. Flood extents of the three hydraulic simulations (Sim 1 = W_5 m; Sim 2 = W_2 m; Sim 3 = W_0.05 m) projected on the same map (separate maps in SM16, SM19, SM21).

Table 3. Area differences (km²) of flood inundated regions between Sim 1 and Sim 3 (W_5 m–W_0.05 m) and Sim 2 and Sim 3 (W_2 m–W_0.05 m) as overall error, overestimations, and underestimations.

Flood Extent Error	Overall Error Area (km ²)	Overestimation Area (km ²)	Overestimation Area (%)	Underestimation Area (km ²)	Underestimation Area (%)
W_5 m vs. W_0.05 m	0.144	0.143	99.31%	0.001	0.69%
W_2 m vs. W_0.05 m	0.242	0.219	90.50%	0.023	9.50%

Table 4. Flood extent and flow depth statistics for the three simulations.

Sim	Flood Extent			Flow Depth	
	Area (km ²)	Algebraic Error (vs. Sim 3; km ²)	Algebraic Error (vs. Sim 3; %)	Min (m)	Max (m)
1	0.836	0.144	17.22%	0.002	5.979
2	0.896	0.242	27.01%	0.002	11.474
3	0.700	-	-	0.002	11.397

As presented in Table 3, the overall flood extent error of free DEM-based Sims (1 and 2) vs. the “ground truth” (Sim 3), expressed as the total area (km²) of overestimation and underestimation, is 70% larger for Sim 2 (0.242 km² or 27.01% of the respective inundation area) compared to Sim 1 (0.242 km² or 17.22% of the respective inundation area). This is rather counter-intuitive: W_5 m is closer to the “ground truth”, whereas W_2 m exhibits extended overestimations (0.219 km²). Moreover, the most alarming result is that, while Sim 1’s error is 99.31% overestimations, and only 0.69% underestimations (area-wise), Sim 2 exhibits 0.023 km² underestimations, approximately 10% of all its errors (Table 3). Examples of serious underestimations are indicated on Figure 9, e.g., in river section 5 (SR = 2.2). These underestimation errors are possibly risky, as they are not on the safe side. Overall, it is observed that there seem to be more errors in the sinuous and especially meandering sections of the river. Particular consideration should be given in areas where tributary streams converge to the main river (see Figure 9); these areas can be mistakenly considered as of greater than the actual importance flood-wise, due to their simulated extensive flooding.

Figure 10 presents the flow depth maps for all Sims side-by-side, whereas Figure 11 presents the flow depth differences between Sim 1 and Sim 3, and Sim 2 and Sim 3, respectively. Whereas Sim 2’s range of flow depths (0.002 m–11.474 m) generally matches the respective range of Sim 3 (0.002 m–11.397 m; Table 4), a closer inspection reveals an inconsistency in their spatial distribution (Figure 10). With that in mind, Sim 1, though generally underestimating the flow depths, is in principle closer to Sim 3, and hydraulically more accurate. This is apparent in Figure 10, as the higher flow depths are positioned on the river centerline in Sim 1 (just like Sim 3). This is not the case for Sim 2, where the flow seems inconsistent and does not follow the real river centerline. Sim 1’s flow depth errors (compared to Sim 3 “ground truth”) range from −9.89 m to +5.85 m, whereas Sim 2’s errors range from −7.47 m to +11.47 m. Sim 1 generally tends to underestimate flow depths up to 33% more than Sim 2, compared to the “ground truth”, whereas Sim 2 tends to overestimate them up to 96% more than Sim 1. Considering the spatial distribution of flow depth errors, Sim 1 overestimates flow depths in a smaller area than Sim 2, while underestimating them in a larger area (Figure 11).

In search of the root of the errors in flood extents and flow depths, the meandering section of the river is selected to be scrutinised, as it is observed to exhibit extreme differences. Figure 12a presents the elevation differences between DTM_5 m and DTM_0.05, whereas Figure 12c presents the resulting flood extents of Sim 1 and Sim 3 (W_5 m and W_0.05 m) together with the flow depth differences between Sim 1 (y_5 m) and Sim 3 (y_0.05 m). In a similar fashion, Figure 12b presents DTM_5 m vs. DTM_0.05, whereas Figure 12d presents the resulting W_5 m and W_0.05 m, together with y_5 m vs. y_0.05 m. Figure 13 presents the locations of the two selected cross-sections, featured in detail in Figure 14.

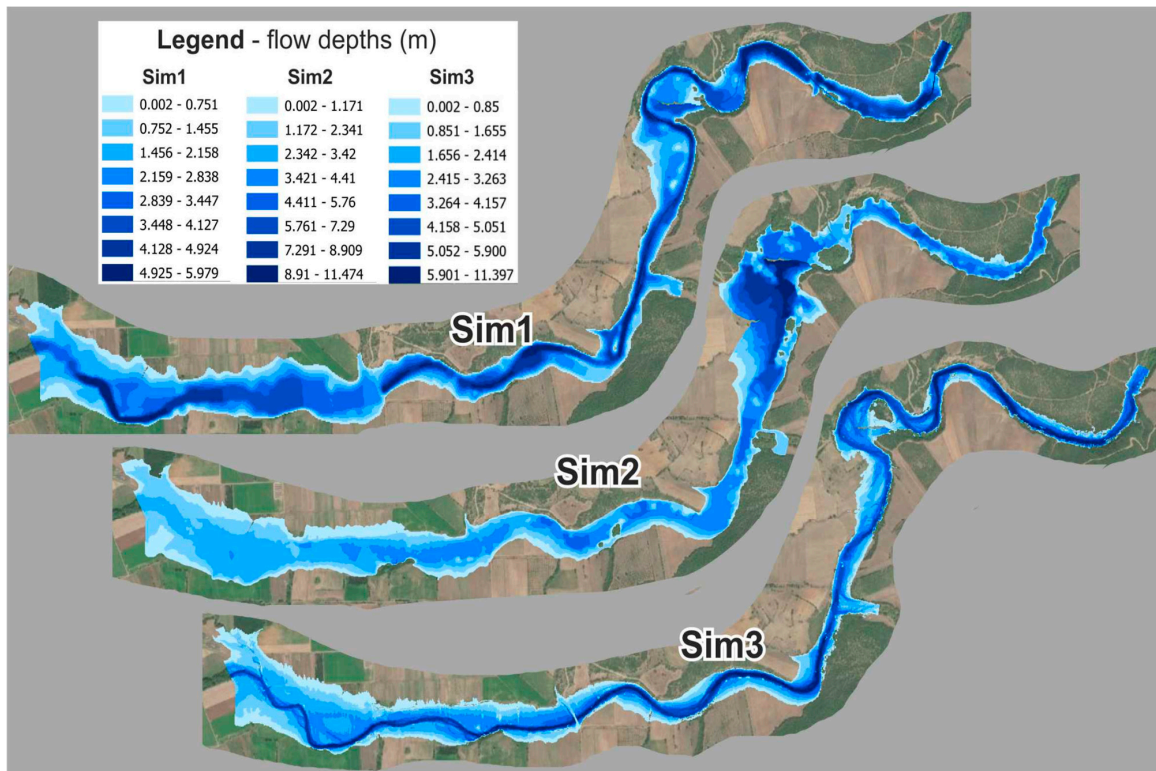


Figure 10. Flow depths of the three hydraulic simulations (Sim 1 = y_5 m; Sim 2 = y_2 m; Sim 3 = $y_{0.05}$ m; for separate hi-res maps see SM17, SM20, SM22).

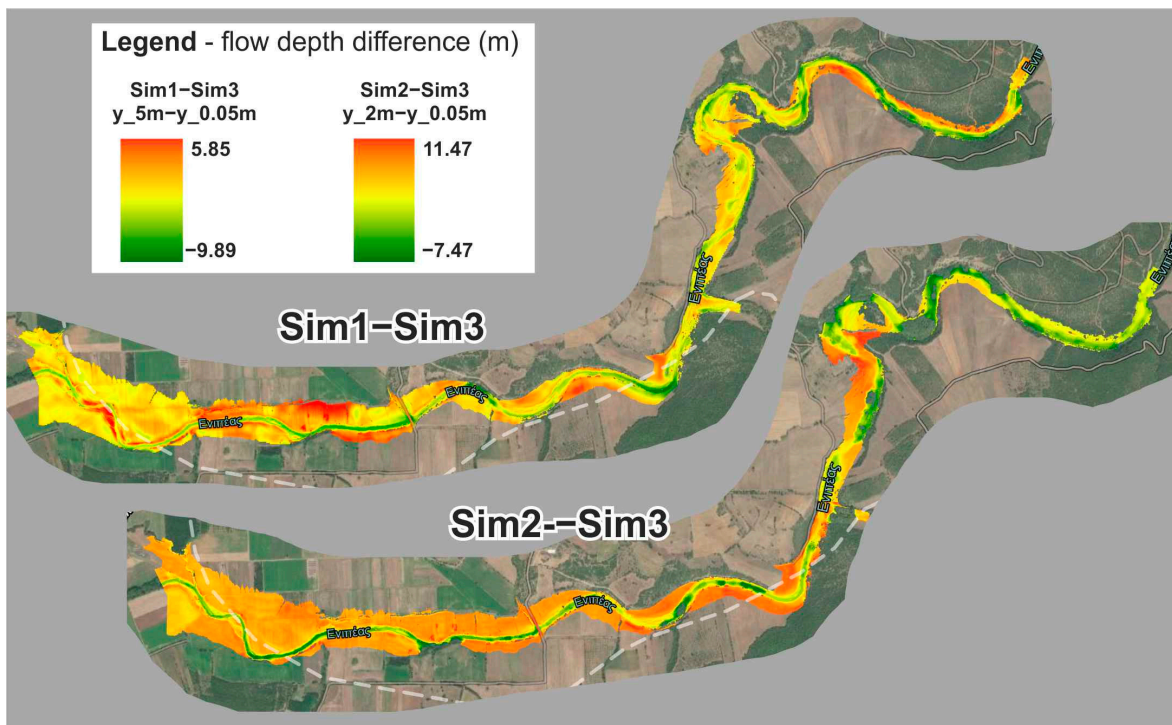


Figure 11. Flow depth differences between Sim 1 and Sim 3 (y_5 m – $y_{0.05}$ m) and Sim 2 and Sim 3 (y_2 m – $y_{0.05}$ m), presented only for the intersection of the respective inundated areas.

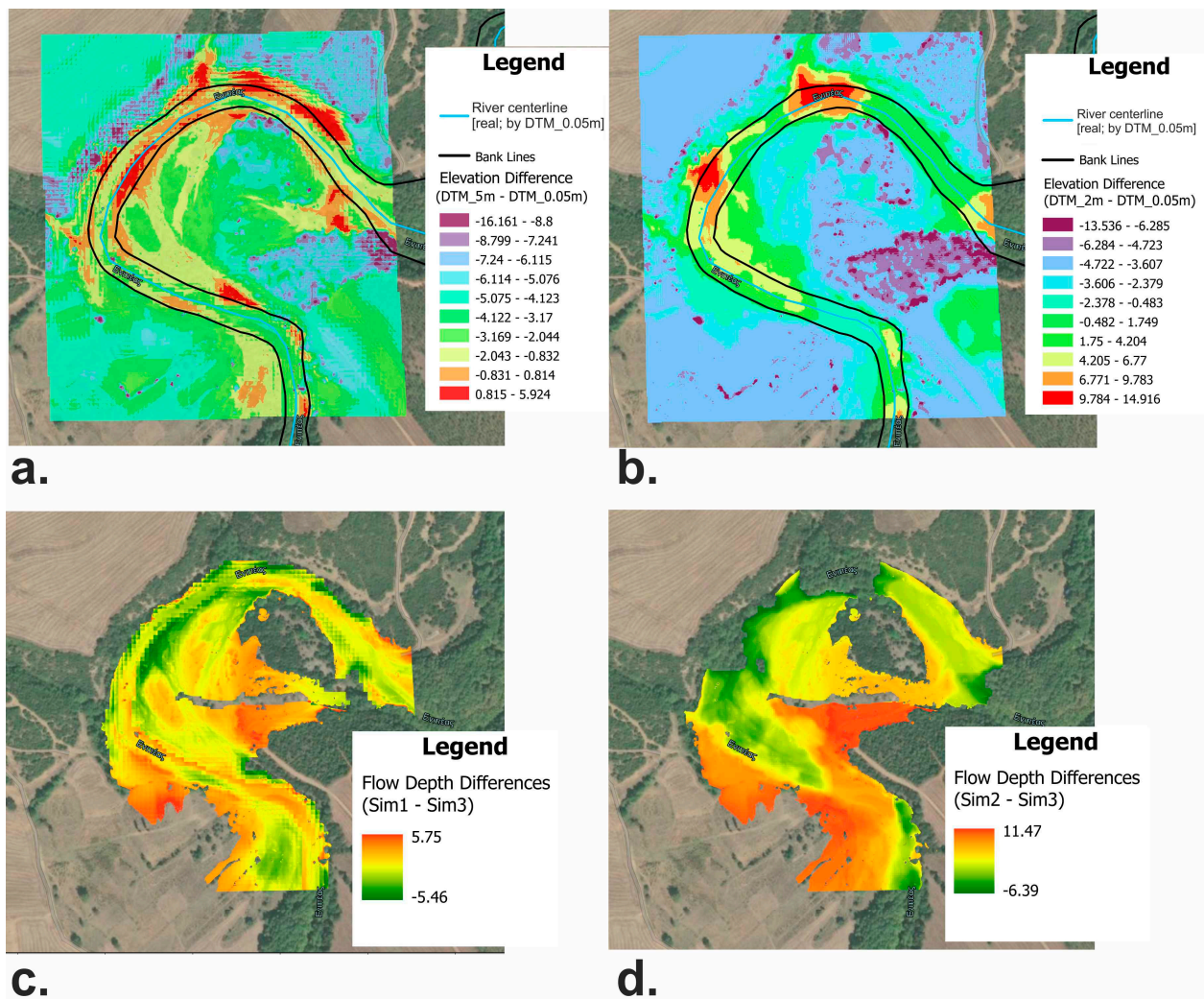


Figure 12. A section of the “flood area” (meandering) presenting differences in elevation (a) DTM_5 m vs. DTM_0.05 m, (b) DTM_2 m vs. DTM_0.05 m and flow depths for (c) Sim 1–Sim 3 and (d) Sim 2–Sim 3.

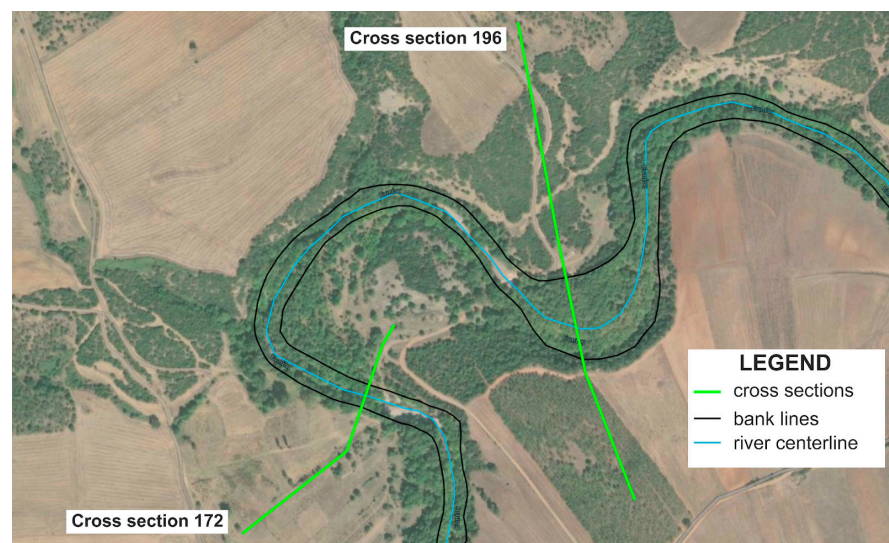


Figure 13. Exact locations of two selected cross-sections (172 and 196; see SM23) in the meandering part of the river in the “flood area”, featured in detail in Figure 14.

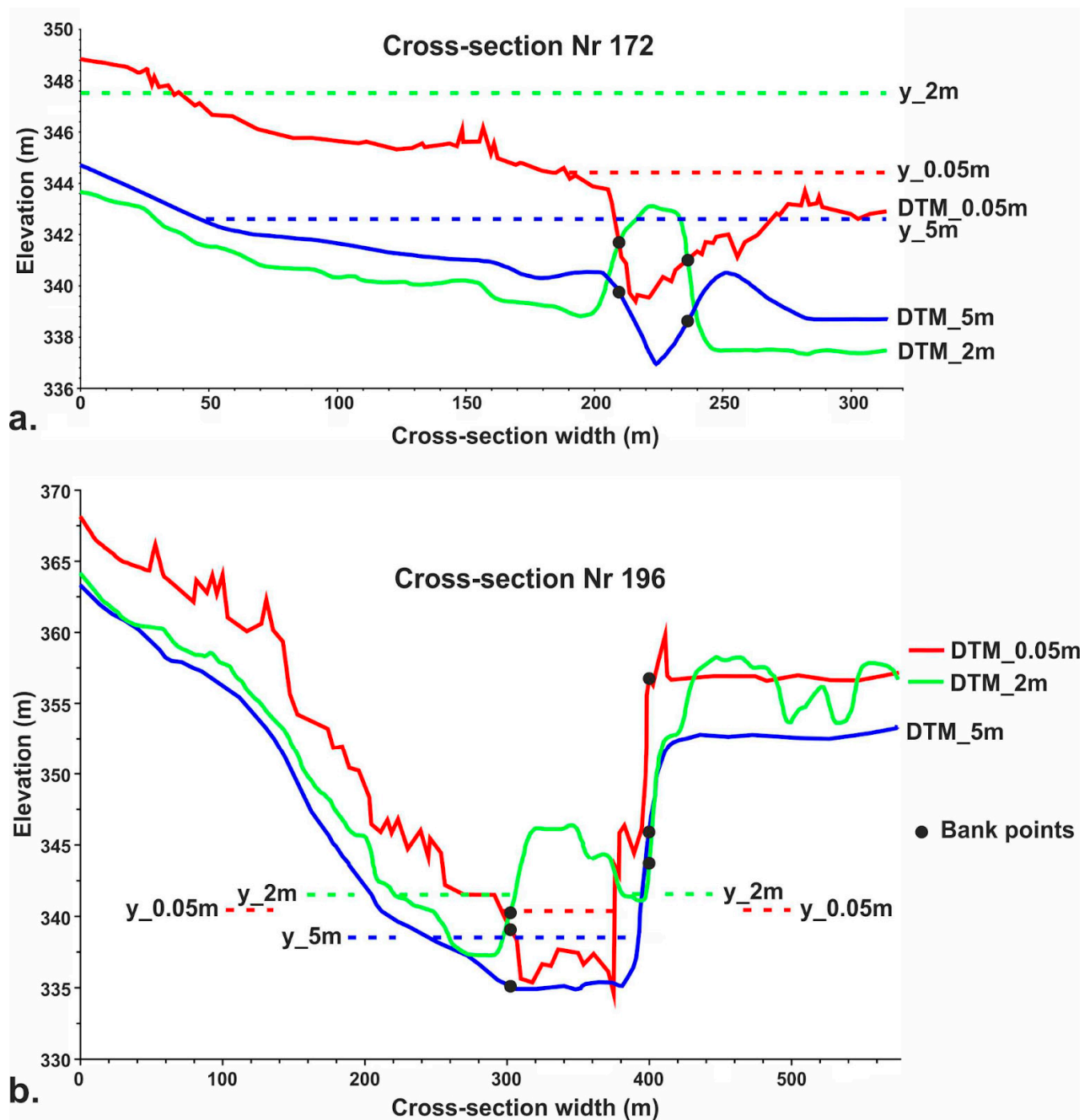


Figure 14. The geometry of the three versions of (a) cross-section 172 and (b) cross-section 196; (see SM23) as derived from DTM_5 m (blue), DTM_2 m (green), and DTM_0.05 m (red). DTM_5 m captures the general geometry, whereas DTM_2 m fails to delineate the main channel.

It is apparent that DTM_5 m exhibits elevation underestimations in most of the surveyed area (Figure 12a). The areas where it overestimates elevation are limited and marginally inside the banks, never on the centerline, hence managing to capture the geometry of the cross-sections (Figure 14). On the other hand, DTM_2 m generally underestimates elevation and overestimates near and inside the banks, even on the centerline, hence being unable to capture the true geometry of the cross sections (Figure 14). This practically results in the altering of the river pathways, as explicitly delineated in Figure 15, that simultaneously presents the river centerlines, as automatically produced based on DTM_5 m, DTM_2 m, and DTM_0.05 m, respectively. Whereas the DTM_5 m-derived centerline is a good approximation of the “ground truth” DTM_0.05 m, the DTM_2 m-derived centerline

exhibits serious deviations, especially along the meandering sections. These errors in the initial topography data propagate and are the root causes of the errors in flood extent and flow depth results (Figure 12c,d). This is also obvious in Figure 14, where the water surface elevations (flow depths; y) vary significantly. A closer look reveals a strong connection of the errors in DTMs with the mapping of dense vegetation and canopy, especially in DTM_2 m, despite the fact that its resolution is in principle higher than DTM_5 m.

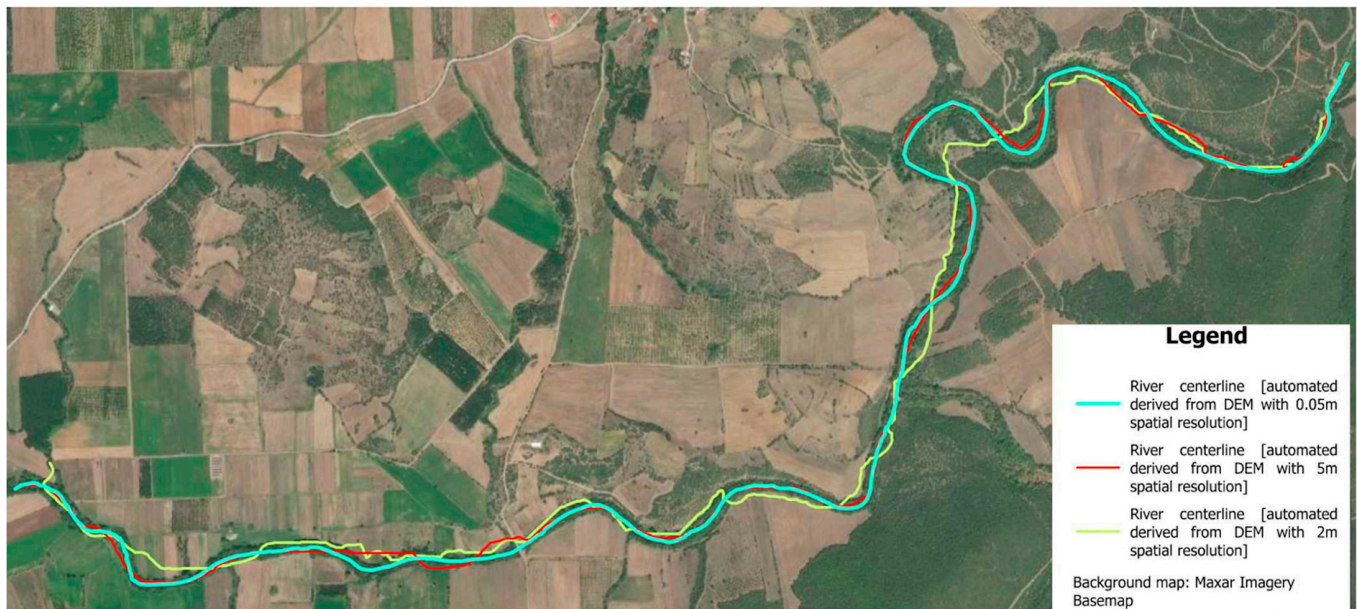


Figure 15. River centerlines derived from the 3 DTMs projected on the same map (see SM30) for comparison purposes. All simulations are based on “ground truth” centerline (by DTM_0.05 m).

3.2. Statistical Analysis Based on Correlation Matrix (Step 13)

The correlation matrix presenting correlation coefficient values between all involved input data and variables (Sim/DTM-specific or common for all Sims/DTMs) and results (flood extents, flow depths, flow characteristics) are presented in Figure 16. The values of interest are highlighted and discussed.

There is an almost linear relationship between riverbed elevations of all DTMs (in relation to the real centerline derived by DTM_0.05 m) and the cross-section ID (consecutive) numbers. The strong linearities are explained by the fact that rivers flow downhill and riverbeds exhibit a positive slope in the vast majority of their length. Hence, the larger the ID number of a cross-section, the lower the respective elevation. Although this is expected, the correlation coefficient values (C_c) are (stronger to weaker correlations) $C_{c_0.05\text{ m}} = -0.99$, $C_{c_5\text{ m}} = -0.98$, and $C_{c_2\text{ m}} = -0.95$. The small variations support the previous findings, indicating better riverbed elevation approximation (compared to the “ground truth” DTM_0.05 m) by DTM_5 m, rather than DTM_2 m.

Another interesting correlation is the relationship between riverbed elevations (Z) and the respective cross-section-specific flood extents (top widths; W). Again, the “ground truth” correlation between $Z_{0.05\text{ m}}$ and $W_{0.05\text{ m}}$ is the highest in value ($C_{c_0.05\text{ m}} = +0.71$), followed by $C_{c_5\text{ m}} = 0.6$ and finally $C_{c_2\text{ m}} = 0.55$. The absolute value of any of the aforementioned C_c is rather random. A finding worth mentioning is the variation in C_c that supports the claim that the closest fit between DTM_5 m and DTM_0.05 m, compared to DTM_2 m, also results in a closest fit between $W_{5\text{ m}}$ and $W_{0.05\text{ m}}$, compared to $W_{2\text{ m}}$. This pattern continues in the relationship between the hydraulic radius values (R), as well as Froude number (Fr), and the respective W for each Sim. Sim 1 results are closer to Sim 3 compared to Sim 2. Specifically, the variation of the impact of R on W concerning Sim 2 is extreme: while $C_{c_0.05\text{ m}} = -0.7$ and $C_{c_5\text{ m}} = -0.53$, $C_{c_2\text{ m}}$ is positive and equal

to +0.39. Finally, the correlations between the flood extents themselves support the main argument: $Cc_5 - 0.05 = +0.82$, $Cc_5 - 2 = +0.81$, and $Cc_2 - 0.05 = +0.71$.

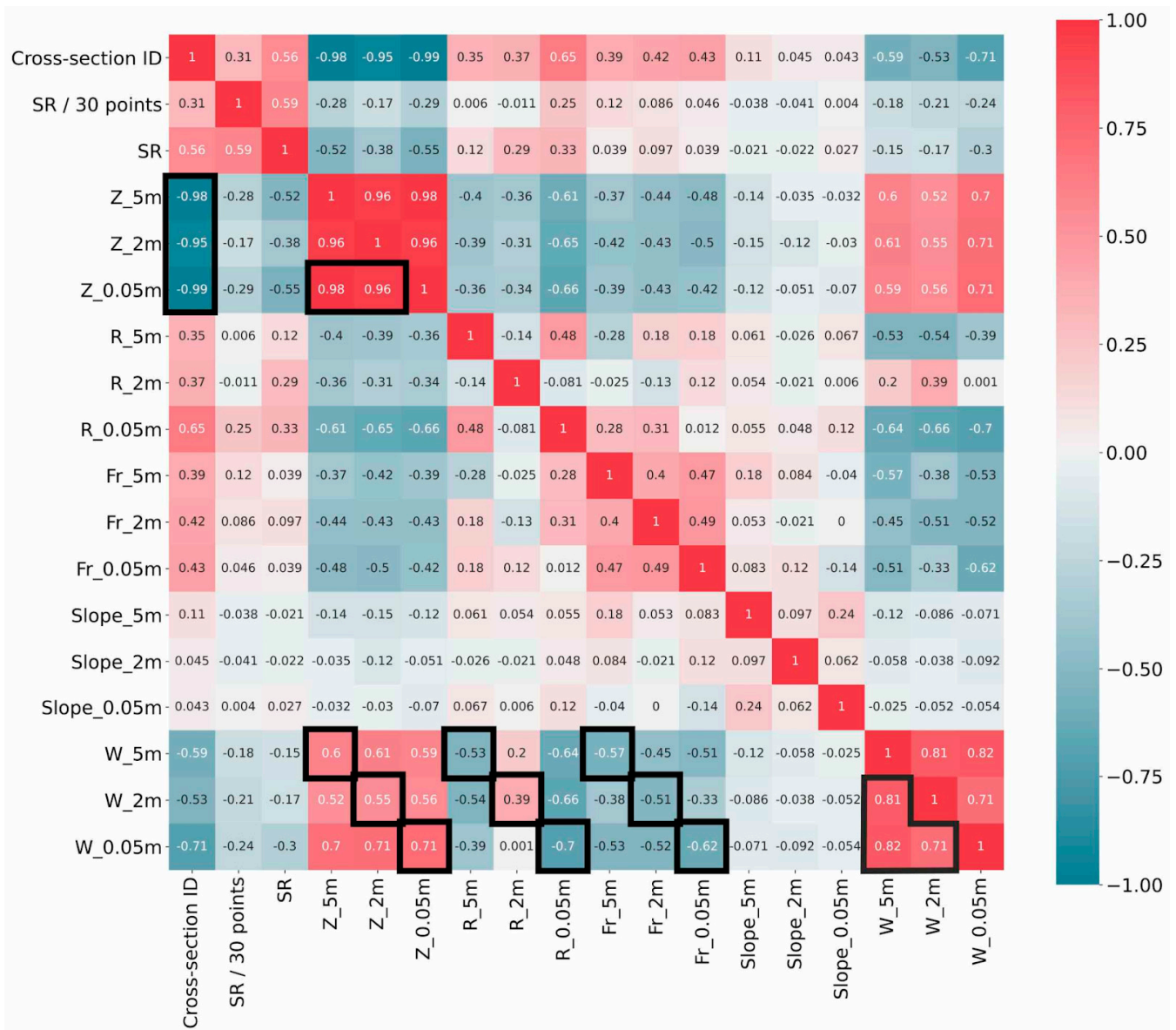


Figure 16. Correlation matrix presenting correlation coefficient values between all involved input data and variables (Sim/DTM-specific or common for all Sims/DTMs) and results (flood extents, flow depths, flow characteristics). Values of interest are highlighted.

3.3. Machine Learning for Interpretation of Nonlinear Relationships (Random Forests)

The histograms of Figure 17 present the distribution of errors of Sim 1 and Sim 2 flood extent errors, compared to Sim 3. The distributions indicate larger errors for Sim 2 compared to Sim 1, and are skewed, also indicating nonlinearities in the error generation and propagation. This is why the method of feature importance calculation using Mean Decrease in Impurity (MDI) is implemented with Random Forest. After a series of tests, the interval (t_{lower} , t_{upper}) is empirically selected as $(-10, +1)$, so that the remaining negative and positive value sets of the distribution are split equally.

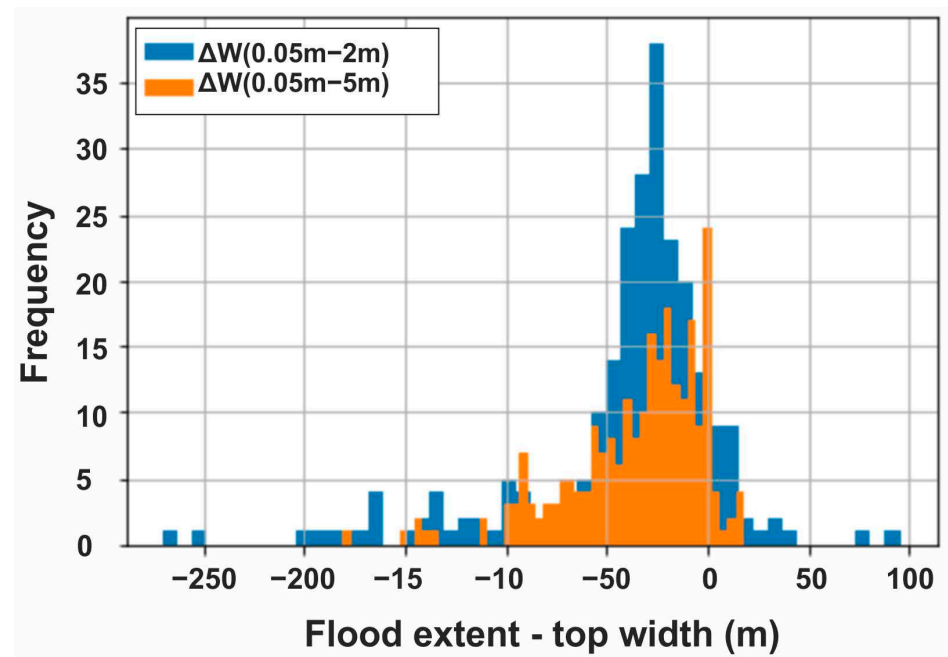


Figure 17. Histograms of the errors of Sim 1 and Sim 2 vs. “ground truth” Sim 3, indicating skewed distributions and nonlinear dependencies.

Following the already presented methodology, using a random noise feature as the “dummy” variable as a means of comparison, the feature importance of the following variables and variable errors regarding their impact on flood extent error ΔW are tested: sinuosity (SR; fixed, see Figure 9), rolling sinuosity (SR/30 sections), error of riverbed elevations (ΔZ), error of hydraulic radii (ΔR), and error of Froude number values (ΔFr). Figure 18 presents the MDI for the aforementioned features. Specifically, Figure 18a presents results for Sim 1 vs. Sim 3 ($W_{0.05\text{ m}}-W_{5\text{ m}}$) and the feature importance of SR, SR/30 sections, $Z_{5\text{ m}}-W_{0.05\text{ m}}$, $R_{5\text{ m}}-R_{0.05\text{ m}}$, and $Fr_{5\text{ m}}-Fr_{0.05\text{ m}}$. Figure 18b presents results for Sim 2 vs. Sim 3 ($W_{0.05\text{ m}}-W_{2\text{ m}}$) and the feature importance of SR, SR/30 sections, $Z_{2\text{ m}}-W_{0.05\text{ m}}$, $R_{2\text{ m}}-R_{0.05\text{ m}}$, and $Fr_{2\text{ m}}-Fr_{0.05\text{ m}}$.

As far as Sim 1 flood extent errors are concerned, SR, ΔR , and ΔFr seem to be equally important. This can be interpreted as follows: the DEM_5 m intrinsic errors propagate up to the flood extent results in the sections of increased sinuosity, driven especially by the resulting errors in the hydraulic radius and Froude number values calculation. On the other hand, Sim 2 flood extent errors’ origin and root cause are different. The feature that stands out is the hydraulic radii of the cross-sections; their importance is far higher than the respective features related to Sim 1 errors. These results fully support the earlier conclusions drawn by the flood maps-based comparative analysis (Step 12) and the correlation matrix-based statistical analysis (Step 13). The hydraulic radii per cross-section are distorted in the main channel in Sim 2, due to the DEM_2 m production process failing to filter dense vegetation.

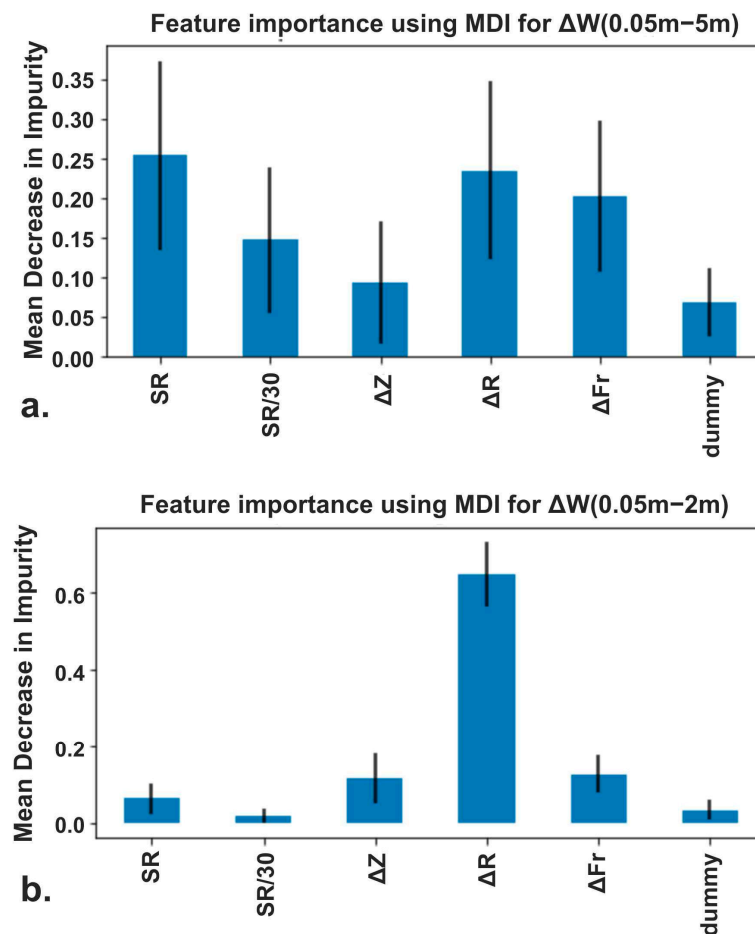


Figure 18. Random Forest-calculated feature importance for fixed sinuosity ratio SR, rolling SR per 30 cross-sections, ΔZ (0.05 m–5 m), ΔR (0.05 m–5 m), ΔFr (0.05 m–5 m), and a dummy variable (random noise) using Mean Decrease in Impurity (MDI) for (a) ΔW (0.05 m–2 m) and (b) ΔW (0.05 m–5 m).

4. Conclusions

This paper investigates flood modelling sensitivity against two sets of open access geospatial elevation data (5 m and 2 m resolution, respectively), derived from the Hellenic Cadastre, and an own designated Unmanned Aerial Vehicle topographical mission (0.05 m resolution). A case study is used concerning a part of the mountainous Enipeas river basin of Thessaly's Water District (Greece).

The first step of the proposed methodology includes a flood maps-based comparative analysis so that experts can empirically draw conclusions on the specific studied river catchment. In the current case study, most of the flood extent errors are overestimations rather than underestimations, at least being on the safe side. Though counter-intuitive, the DEM_5 m-derived (Sim 1) flood extents are closer to the "ground truth", whereas DEM_2 m-derived (Sim 2) extents are extensively overestimated, while also exhibiting relatively alarmingly high underestimations, which are not on the safe side and can have potentially catastrophic implications if used for design purposes. The sections of increased sinuosity ratio, especially the meandering river sections, seem more prone to flood modelling errors. The same applies for junctions of the main channel with modelled, or not, tributary streams. Concerning flow depth results, Sim 1 generally underestimates them and is, in principle, closer to DEM_0.05 m-derived Sim 3, and hydraulically more accurate. The reason is that, although Sim 2 range of flow depths is generally correct, their spatial distribution is inconsistent, as is the flow that does not follow the real river centerline.

The root of the errors concerning flood extents and flow depths lies in the topography data used. DEM_5 m mostly underestimates elevation, but manages to capture the

geometry of the cross-sections, whereas DEM_2 m generally underestimates, but overestimates inside the critical zone of the main channel, near and inside the banks, even on the centerline; it is unable to capture the true geometry of the cross sections, practically altering the river pathways. This is more intense in the meandering river sections. The map-based analysis indicates that the true cause is the inability of DEM_2 m to capture the elevation of the ground in areas of dense vegetation and canopy, usually being wider in the meandering river sections. In absence of detailed information concerning the surveying process followed by the Hellenic Cadastre, and specifically the classification and filtering of the vegetation (tree removal), one can only speculate on the true source of this error. On the other hand, DEM_5 m, though constituting a lower resolution product, seems more suitable for approximating the real terrain.

The flood modelling results are also analysed via a statistical analysis, based on the correlation matrix presenting linear relationships between input data variables (i.e., elevation, slope, sinuosity ratio) and cross section-specific results, including flow characteristics (i.e., Froude number, hydraulic radius), flood extents, and flow depths. The correlation results indicate strong linearities where expected (riverbed elevations vs. cross-section ID numbers), and weaker where expected (i.e., riverbed elevations and hydraulic radii and Froude number vs. flood extents). Nevertheless, the important finding the statistical analysis has to offer is the quantifiable proof of the superiority of DEM_5 m-derived Sim 1 compared to the DEM_2 m-derived Sim 2 results, which supports the preceding empirical analysis conclusions. This is suggested by the fact that correlations of the analysed variables and flood extent results constantly follow the classification (stronger-to-weaker) Sim 3 > Sim 1 > Sim 2. The simple comparison between the correlation of the cross section-specific flood extents of Sim 1–Sim 3 and Sim 2–Sim 3 also supports the argument.

As the conventional approaches fail to identify the nonlinear dependencies of the root cause analysis and error propagation tracking side of the research problem, the proposed methodology finally implements a more sophisticated Machine Learning (ML) analysis, specifically Random Forest importance. The ML approach results further support and solidify the earlier conclusions drawn by the flood maps-based comparative analysis and the correlation matrix-based statistical analysis. The failure of the DEM_2 m production process to map the terrain in areas of dense vegetation and wide canopy leads to unreal cross-section geometries and inserts critical errors in the respective hydraulic radii, really important at least in 1D hydraulic analyses. These errors further propagate to the flood extent results, as the RF importance approach robustly indicates.

As far as the general proposed methodology is concerned, for deciding the best available alternative DEM of an accurate but costly UAV-based or in situ ground survey-based DEM, no step is redundant. The flood map-based comparative analysis by experts is the main and key evaluation tool and cannot be replaced by a statistical or even a more sophisticated Machine Learning-based analysis. Machine Learning methods can interpret nonlinear dependencies but depend on the way they are implemented and are susceptible to parameter errors. Nevertheless, they provide further insight on the root and cause of the error and the propagation mechanism, while identifying additional error patterns. The proposed stages and steps should be implemented as an integrated methodology.

The conclusions of the current paper and related research can be summed up as steps of a suggested procedure for the optimal hydraulic simulation of a river basin, in terms of minimisation of in situ topographical mapping costs without compromising the hydraulic simulation accuracy:

1. Approximate the real river centerline, as accurately as possible, utilising any available source and technique possible. A realistic approach would be the use of the most recent and high resolution open-source DEM available, in order to automatically produce an approximate river centerline, calibrated by recent satellite imagery (e.g., google earth) and orthophotos (e.g., Hellenic Cadastre in Greek reality), supported by in situ inspection if possible or necessary.

2. In river areas exhibiting one or more of the following characteristics: (a) dense vegetation or/and wide canopy, (b) meandering sections, (c) junctions of the main channel with tributary streams, or/and generally (d) centerline-bank lines derived from the available DEM diverging from the real centerline-bank lines, proceed to UAV-based mapping (combined with an a-posteriori vegetation removal process) or in situ topographical ground surveying.
3. In areas not belonging to the previous category, if more than one open-source DEM is available, the implemented and proposed methodology of this paper should be followed in order to select the one that inserts and propagates less errors in the hydraulic simulations. In Greek reality, just use the DEM_5 m by Hellenic Cadastre, as it is proven to be more efficient for, at least 1D, hydraulic simulations, rather than the higher resolution DEM_2 m.
4. Future research should include more case studies of different terrain characteristics, such as sinuosity, lush and weak vegetation areas, etc., combined with real in situ topographical ground surveying and validated flood extents and flow depth measurements. The larger datasets will also provide further credibility to the Machine Learning-based analysis. In the proposed methodology, 2D hydraulic simulations (e.g., using HEC-RAS 2D) should be tested to check their sensitivity vs. the various spatial resolution DEMs. Finally, more sophisticated ML techniques, such as Gradient Boost Algorithms, Fuzzy Cognitive Maps, and Self Organizing Maps, can be used for root cause analysis.

Author Contributions: Conceptualization, N.X., Y.K. and E.F.; methodology, N.X., Y.K., E.F. and K.P.; software, N.X., Y.K., E.F. and K.P.; validation, N.X., Y.K., E.F. and K.P.; investigation, N.X., Y.K., E.F. and K.P.; resources, N.X., Y.K. and E.F.; data curation, N.X., Y.K. and E.F.; writing—original draft preparation, N.X., Y.K., E.F. and K.P.; writing—review and editing, N.X., Y.K., E.F., S.K., N.A., D.D. and K.K.; visualization, N.X., Y.K. and K.P.; supervision, E.F., S.K., N.A. and K.K.; project administration, N.X., Y.K. and E.F. All authors have read and agreed to the published version of the manuscript.

Funding: This research received no external funding.

Data Availability Statement: Data supporting the reported results can be found at: https://drive.google.com/drive/folders/1L6_Whis8PSO5ArZjJT375CINRMYPMNt?usp=share_link (accessed on 26 February 2023).

Conflicts of Interest: The authors declare no conflict of interest.

Appendix A

The supporting information presented in detail in Table A1 of Appendix A, can be downloaded at: https://drive.google.com/drive/folders/1L6_Whis8PSO5ArZjJT375CINRMYPMNt?usp=share_link (accessed on 26 February 2023).

Table A1 presents the list and relevant information concerning the Appendix A referred to in the text.

Table A1. List of Appendix A and relevant information.

Nr	Product	Filename	Description
SM1	P1a	SM1-(P1a) DTM5 m flood.pdf	Map of the DTM_5 m covering only the “flood area”, derived from DEM_5 m by Hellenic Cadastre open data, only covering the “flood area”.
SM2a	P1b_hydro	SM2a-(P1b_hydro) DTM2 m hydro.pdf	Map of the DTM_5 m covering the full “hydro area” derived from DEM_2 m by Hellenic Cadastre open data.

Table A1. Cont.

Nr	Product	Filename	Description
SM2b	P1b_flood	SM2b-(P1b_flood) DTM2 m flood.pdf	Map of the DTM_5 m covering only the “flood area”, derived from DEM_2 m by Hellenic Cadastre open data.
SM3	P1c	SM3-(P1c) DTM0.05 m.pdf	Map of the DTM_0.05 m derived from a research team’s UAV survey mission in the “flood area”.
SM4	P2a	SM4-(P2a) subcatchments.pdf	Map of the 6 sub-catchments’ delineation.
SM5	P2b	SM5-(P2b) hydrographic network.pdf	Map of the hydrographic network in the “hydro area” derived by RBMP [27].
SM6a	P2c	SM6a-(P2c) river centerline by DTM0.05 m.pdf	Map of the river centerline, derived from DEM_0.05 m, in the delineated “flood area”.
SM6b	P2c_DTM	SM6b-(P2c_DTM) river centerline by DTM0.05 m on DTM.pdf	Map of the river centerline, derived from DEM_0.05 m, on the respective DTM in the delineated “flood area”.
SM7a	P2d	SM7a-(P2d) river centerline by DTM2 m.pdf	Map of the river centerline, derived from DEM_2 m, in the delineated “flood area”.
SM7b	P2d_DTM	SM7b-(P2d_DTM) river centerline by DTM2 m on DTM.pdf	Map of the river centerline, derived from DEM_2 m, on the respective DTM in the delineated “flood area”.
SM8a	P2e	SM8a-(P2e) river centerline by DTM5 m.pdf	Map of the river centerline, derived from DEM_5 m, in the delineated “flood area”.
SM8b	P2e_DTM	SM8a-(P2e_DTM) river centerline by DTM5 m on DTM.pdf	Map of the river centerline, derived from DEM_5 m, on the respective DTM in the delineated “flood area”.
SM9	P2f + P7	SM9-(P2f + P7) geomorphology + time conc. + time lags.xlsx	An excel file presenting the sub-catchment characteristics and the respective calculations.
SM10	P3a	SM10-(P3a) soil data map	A soil data map presenting the available soil data concerning the “hydro area”, derived from [34].
SM11	P3b	SM11-(P3b).pdf hydrolithological map.pdf	A hydrolithological map presenting the drainage characteristics of the “hydro area”, derived from the respective soil data (SM11; [34]), where available, and [27] in the remaining areas.
SM12	P4	SM12-(P4) land uses map.pdf	A land uses map of the “hydro area”, derived from CORINE [35].
SM13	P5	SM13-(P5) 6 hyetographs.xlsx	An excel file presenting the hyetographs per sub-catchment based on the Anavra station IDF curve using the Alternate Block Method [42,43].
SM14	P6	SM14-(P6) Land cover and CN per subcatchment.xlsx	An excel file presenting the CNc estimations per sub-catchments with the respective calculations.
SM15	P8	SM15-(P8) 9 hydrographs.pdf	A pdf file with the 9 hydrographs (3 hydrographs for the 3 junctions and 6 for the 6 sub-catchments) produced during Step 8 of Stage 2.
SM16	P9a	SM16-(P9a) flood extents map W_5 m.pdf	Map of the flood extents simulated by Sim 1 with the automatically derived centerline by the respective DTM_5 m.
SM17	P9b	SM17-(P9b) flow depths map y_5 m.pdf	Map of the flow depths simulated by Sim 1 with the automatically derived centerline by the respective DTM_5 m.

Table A1. Cont.

Nr	Product	Filename	Description
SM18	P9c + P10c + P11c	SM18-(P9c + P10c + P11c) flow characteristics.xlsx	An excel file presenting the selected flow characteristics for all Sims (fc_5 m, fc_2 m, fc_0.05 m).
SM19	P10a	SM19-(P10a) flood extents map W_2 m.pdf	Map of the flood extents simulated by Sim 2 with the automatically derived centerline by the respective DTM_2 m.
SM20	P10b	SM20-(P10b) flow depths map y_2 m.pdf	Map of the flow depths simulated by Sim 2 with the automatically derived centerline by the respective DTM_2 m.
SM21	P11a	SM21-(P11a) flood extents map W_0.05 m.pdf	Map of the flood extents simulated by Sim 3 with the automatically derived centerline by the respective DTM_0.05 m.
SM22	P11b	SM22-(P11b) flow depths map y_0.05 m.pdf	Map of the flow depths simulated by Sim 3 with the automatically derived centerline by the respective DTM_0.05 m.
SM23	-	SM23-Map with cross-sections.pdf	A pdf file presenting all 270 cross-sections of the flood area created in an interval of 20 m
SM24	P9a + P10a + P11a	SM24-(P9a + P10a + P11a) flood extents maps.pdf	Map of all simulated flood extents (W_5 m, W_2 m, W_0.05 m).
SM25	P9a vs. P11a	SM25-(P9a + P11a) flood extents maps.pdf	Map of simulated flood extents of Sim 1 and Sim 3 (W_5 m vs. W_0.05 m).
SM26	P10a vs. P11a	SM26-(P10a + P11a) flood extents maps.pdf	Map of simulated flood extents of Sim 2 and Sim 3 (W_2 m vs. W_0.05 m).
SM27	P9a vs. P10a	SM27-(P9a + P10a) flood extents maps.pdf	Map of simulated flood extents of Sim 1 and Sim 2 (W_5 m vs. W_2 m).
SM28	-	SM28-DTM5 m-DTM0.05 m.pdf	Map of elevation differences between DTM_5 m and DTM_0.05 m in a selected meandering section of the river.
SM29	-	SM29-DTM2 m-DTM0.05 m.pdf	Map of elevation differences between DTM_2 m and DTM_0.05 m in a selected meandering section of the river.
SM30	-	SM30-all river centerlines.pdf	Map of all three centerlines derived from the respective DEM.
SM31	-	SM31-y_5 m-y_0.05 m.pdf	Map of flow depth differences between Sim 1 and Sim 3 (y_5 m-y_0.05 m).
SM32	-	SM32-y_2 m-y_0.05 m.pdf	Map of flow depth differences between Sim 2 and Sim 3 (y_2 m-y_0.05 m).

References

1. Talbot, C.J.; Bennett, E.M.; Cassell, K.; Hanes, D.M.; Minor, E.C.; Paerl, H.; Raymond, P.A.; Vargas, R.; Vidon, P.G.; Wollheim, W.; et al. The Impact of Flooding on Aquatic Ecosystem Services. *Biogeochemistry* **2018**, *141*, 439–461. [[CrossRef](#)] [[PubMed](#)]
2. Yu, Q.; Wang, Y.; Li, N. Extreme Flood Disasters: Comprehensive Impact and Assessment. *Water* **2022**, *14*, 1211. [[CrossRef](#)]
3. Rotunno, R.; Houze, R.A. Lessons on Orographic Precipitation from the Mesoscale Alpine Programme. *Q. J. R. Meteorol. Soc.* **2007**, *133*, 811–830. [[CrossRef](#)]
4. Borga, M.; Stoffel, M.; Marchi, L.; Marra, F.; Jakob, M. Hydrogeomorphic Response to Extreme Rainfall in Headwater Systems: Flash Floods and Debris Flows. *J. Hydrol.* **2014**, *518*, 194–205. [[CrossRef](#)]
5. Lumbroso, D.; Gaume, E. Reducing the Uncertainty in Indirect Estimates of Extreme Flash Flood Discharges. *J. Hydrol.* **2012**, *414–415*, 16–30. [[CrossRef](#)]
6. Ashley, S.T.; Ashley, W.S. Flood Fatalities in the United States. *J. Appl. Meteorol. Climatol.* **2008**, *47*, 805–818. [[CrossRef](#)]
7. Diakakis, M.; Deligiannakis, G. Flood Fatalities in Greece: 1970–2010. *J. Flood Risk Manag.* **2015**, *10*, 115–123. [[CrossRef](#)]

8. Diakakis, M.; Deligiannakis, G.; Katsetsiadou, K.; Antoniadis, Z.; Melaki, M. Mapping and Classification of Direct Flood Impacts in the Complex Conditions of an Urban Environment. The Case Study of the 2014 Flood in Athens, Greece. *Urban Water J.* **2017**, *14*, 1065–1074. [CrossRef]
9. Merz, B.; Kreibich, H.; Schwarze, R.; Thieken, A. Review Article “Assessment of Economic Flood Damage”. *Nat. Hazards Earth Syst. Sci.* **2010**, *10*, 1697–1724. [CrossRef]
10. Barredo, J.I. Normalised Flood Losses in Europe: 1970–2006. *Nat. Hazards Earth Syst. Sci.* **2009**, *9*, 97–104. [CrossRef]
11. Gaume, E.; Bain, V.; Bernardara, P.; Newinger, O.; Barbuc, M.; Bateman, A.; Blaškovičová, L.; Blöschl, G.; Borga, M.; Dumitrescu, A.; et al. A Compilation of Data on European Flash Floods. *J. Hydrol.* **2009**, *367*, 70–78. [CrossRef]
12. Tegos, A.; Ziogas, A.; Bellos, V.; Tzimas, A. Forensic hydrology: A complete reconstruction of an extreme flood event in data-scarce area. *Hydrology* **2022**, *9*, 93. [CrossRef]
13. Bellos, V.; Kourtis, I.; Raptaki, E.; Handrinos, S.; Kalogiros, J.; Sibetheros, I.A.; Tsihrintzis, V.A. Identifying Modelling Issues through the Use of an Open Real-World Flood Dataset. *Hydrology* **2022**, *9*, 194. [CrossRef]
14. Jongman, B. Effective Adaptation to Rising Flood Risk. *Nat. Commun.* **2018**, *9*, 1986. [CrossRef] [PubMed]
15. Dimitriadis, P.; Tegos, A.; Oikonomou, A.; Pagana, V.; Koukouvinos, A.; Mamassis, N.; Koutsoyiannis, D.; Efstratiadis, A. Comparative evaluation of 1D and quasi-2D hydraulic models based on benchmark and real-world applications for uncertainty assessment in flood mapping. *J. Hydrol.* **2016**, *534*, 478–492. [CrossRef]
16. Hawker, L.; Bates, P.; Neal, J.; Rougier, J. Perspectives on Digital Elevation Model (DEM) Simulation for Flood Modeling in the Absence of a High-Accuracy Open Access Global Dem. *Front. Earth Sci.* **2018**, *6*, 233. [CrossRef]
17. Hellenic Cadastre. Available online: <https://www.ktimatologio.gr> (accessed on 28 January 2023).
18. US Army Corps of Engineers. Available online: <https://www.usace.army.mil> (accessed on 10 January 2023).
19. Ras Mapper User’s Manual. Available online: <https://www.hec.usace.army.mil/confluence/rasdocs/rmum/latest> (accessed on 25 January 2023).
20. HEC-RAS 1D—Hydrologic Engineering Center—River Analysis System. Available online: <https://www.hec.usace.army.mil/software/waterquality/hec-ras.aspx> (accessed on 20 December 2022).
21. Official Government Gazette (O.G.G) of the Hellenic Republic. *Approving the River Basin Management Plan of the River Basins of Thessalia Water District*; No. 2561/B/25.09.14; National Printing Office of Greece: Athens, Greece, 2014.
22. Digital Elevation Model (DEM) for the LSO Project (5m). Available online: <http://gis.ktimanet.gr/geoportal/catalog/search/resource/details.page?uuid=%7B456CB655-B899-450A-87BF-8322B8FB8370%7D> (accessed on 28 January 2023).
23. Digital Elevation Model (DEM) for the LSO25 Ortho Mapping Production (2m). Available online: <https://www.ktimanet.gr/geoportal/catalog/search/resource/details.page?uuid=%7B86CABAFD-00B8-41D4-B36A-2FE8E2DCF958%7D> (accessed on 28 January 2023).
24. Anders, N.; Valente, J.; Masselink, R.; Keesstra, S. Comparing Filtering Techniques for Removing Vegetation from UAV-Based Photogrammetric Point Clouds. *Drones* **2019**, *3*, 61. [CrossRef]
25. Agisoft Metashape. Available online: <https://www.agisoft.com/downloads/user-manuals/> (accessed on 2 February 2023).
26. ESRI ArcGIS Pro. Available online: <https://www.esri.com/en-us/arcgis/products/arcgis-pro/resources> (accessed on 10 October 2022).
27. River Basin Management Plan (RBMP)—EL08 Water District of Thessaly. Available online: <http://wfdver.ypeka.gr/en/management-plans-en/approved-management-plans-en/gr08-approved-en/> (accessed on 10 October 2022).
28. European Union. Water Framework Directive (WFD) 2000/60/EC, 2000. Available online: https://environment.ec.europa.eu/topics/water/water-framework-directive_en (accessed on 26 February 2023).
29. Giandotti, M. *Previsione Delle Piene e Delle Magre dei Corsi D’acqua*; Istituto Poligrafico dello Stato: Rome, Italy, 1934; pp. 107–117.
30. European Soil Data Centre (ESDAC). European Commission, Joint Research Centre. Available online: <https://esdac.jrc.ec.europa.eu> (accessed on 12 December 2022).
31. Panagos, P.; Van Liedekerke, M.; Jones, A.; Montanarella, L. European Soil Data Centre: Response to European Policy Support and Public Data Requirements. *Land Use Policy* **2012**, *29*, 329–338. [CrossRef]
32. Toth, G.; Jones, A.; Montanarella, L. *LUCAS Topsoil Survey. Methodology, Data and Results*; JRC Technical Reports; EUR26102—Scientific and Technical Research series; Publications Office of the European Union: Copenhagen, Denmark, 2013.
33. Jones, A.; Fernandes-Ugalde, O.; Scarpa, S.; Eiselt, B. *LUCAS 2022, EUR 30331 EN*; Publications Office of the European Union: Copenhagen, Denmark, 2022.
34. OPEKEPE—Payment and Control Agency for Guidance and Guarantee Community Aid. *Soil Map of Greece, Scale 1:30,000*; Aristotle University of Thessaloniki: Thessaloniki, Greece, 2015.
35. Corine Land Cover. Available online: <https://land.copernicus.eu/pan-european/corine-land-cover> (accessed on 10 October 2022).
36. Koutsoyiannis, D.; Markonis, Y.; Koukouvinos, A.; Papalexioiu, S.; Mamassis, N.; Dimitriadis, P. Hydrological Study of Severe Rainfall in the Kephisos Basin, Greece, Study of the Management of Kephisos, Commissioner: General Secretariat of Public Works—Ministry of Environment, Planning and Public Works, Contractors: Exarhou Nikolopoulos Bensasson, Denco, G. Karavokiris; et al., 154 Pages, Athens. 2010. Available online: <http://www.itia.ntua.gr/el/docinfo/970/> (accessed on 26 February 2023).
37. Intensity Duration Frequency Curves (IDF) Report. Available online: https://floods.ypeka.gr/egyFloods/IDF/IDF_Report_V4.pdf (accessed on 12 December 2022).

38. Koutsoyiannis, D.; Kozonis, D.; Manetas, A. A mathematical framework for studying rainfall intensity-duration-frequency relationships. *J. Hydrol.* **1998**, *206*, 118–135. [[CrossRef](#)]
39. Veneziano, D.; Langousis, A. The areal reduction factor: A multifractal analysis. *Water Resour. Res.* **2005**, *41*, W07008. [[CrossRef](#)]
40. Koutsoyiannis, D. *Statistical Hydrology*, 4th ed.; National Technical University of Athens: Athens, Greece, 1997; 312p.
41. Collier, C.G.; Hardaker, P.J. Estimating Probable Maximum Precipitation Using a Storm Model Approach. *J. Hydrol.* **1996**, *183*, 277–306. [[CrossRef](#)]
42. Chow, V.T.; Maidment, D.R.; Mays, L.W. *Applied Hydrology*; McGraw-Hill Professional: New York, NY, USA, 1988.
43. Efstratiadis, A.; Koussis, A.D.; Koutsoyiannis, D.; Mamassis, N. Flood Design Recipes vs. Reality: Can Predictions for Ungauged Basins Be Trusted? *Nat. Hazards Earth Syst. Sci.* **2014**, *14*, 1417–1428. [[CrossRef](#)]
44. Soil Conservation Service. *SCS National Engineering Handbook, Section 4, Hydrology*; Govt. Print. Off.: Washington, DC, USA, 1972.
45. Koutsoyiannis, D.; Xanthopoulos, T.H. *Engineering Hydrology*, 3rd ed.; National Technical University of Athens: Athens, Greece, 1999; 418p.
46. Wanielista, M.; Kersten, R.; Eaglin, R. *Hydrology: Water Quantity and Quality Control*; Wiley: New York, NY, USA, 1997.
47. Brunner, G.W. *HEC-Ras River Analysis System: User's Manual*; US Army Corps of Engineers, Hydrologic Engineering Center: Davis, CA, USA, 2021.
48. Brunner, G.W. *HEC-Ras River Analysis System: Hydraulic Reference Manual*; US Army Corps of Engineers, Institute for Water Resources, Hydrologic Engineering Center: Davis, CA, USA, 2021.
49. Auret, L.; Aldrich, C. Interpretation of nonlinear relationships between process variables by use of random forests. *Miner. Eng.* **2012**, *35*, 27–42. [[CrossRef](#)]

Disclaimer/Publisher's Note: The statements, opinions and data contained in all publications are solely those of the individual author(s) and contributor(s) and not of MDPI and/or the editor(s). MDPI and/or the editor(s) disclaim responsibility for any injury to people or property resulting from any ideas, methods, instructions or products referred to in the content.